Available online at www.sciencedirect.com

ScienceDirect

Nuclear Physics B 932 (2018) 471–504

NUCLEAR PHYSICS B

www.elsevier.com/locate/nuclphysb

Muon-to-electron conversion in mirror fermion model with electroweak scale non-sterile right-handed neutrinos

P.Q. Hung [a,b], Trinh Le [a], Van Que Tran [c], Tzu-Chiang Yuan [d,e,*]

[a] *Department of Physics, University of Virginia, Charlottesville, VA 22904-4714, USA*
[b] *Center for Theoretical and Computational Physics, Hue University College of Education, Hue, Viet Nam*
[c] *Department of Physics, National Taiwan Normal University, Taipei 116, Taiwan*
[d] *Institute of Physics, Academia Sinica, Nangang, Taipei 11529, Taiwan*
[e] *Physics Division, National Center for Theoretical Sciences, Hsinchu, Taiwan*

Received 7 February 2018; received in revised form 19 April 2018; accepted 25 May 2018
Available online 30 May 2018
Editor: Hong-Jian He

Abstract

The muon-to-electron conversion in aluminum, titanium and gold nuclei is studied in the context of a class of mirror fermion model with non-sterile right-handed neutrinos having masses at the electroweak scale. We show that the electric and magnetic dipole operators from the photon exchange diagrams provide the dominant contributions, which enables us to derive a simple formula to relate the conversion rate with the on-shell radiative decay rate of muon into electron at the limit of zero momentum transfer and large mirror lepton masses. Current experimental limits (SINDRUM II) and projected sensitivities (Mu2e, COMET and PRISM) for the muon-to-electron conversion rates in various nuclei and latest limit from MEG for the radiative decay rate of muon into electron are used to put constraints on the parameter space of the model. Sensitivities to the new Yukawa couplings can reach the range of one tenth to one hundred-thousandth, depending on the mixing scenarios and mirror fermion masses in the model as well as the nuclei targets used in future experiments.

* Corresponding author.
E-mail addresses: pqh@virginia.edu (P.Q. Hung), amyleo.ntrinh@gmail.com (T. Le), apc.tranque@gmail.com (V.Q. Tran), tcyuan@phys.sinica.edu.tw (T.-C. Yuan).

https://doi.org/10.1016/j.nuclphysb.2018.05.020

1. Introduction

As is well known, lepton flavor is an accidental conserved quantity in Standard Model (SM) with strictly massless neutrinos. For example, a muon never decays radiatively into an electron plus a photon and neutrinos do not oscillate in the SM. However various experiments have now established firmly that neutrinos do oscillate from one flavor to another. The common wisdom, motivated by the physics of $K - \overline{K}$ oscillation in the kaon system, is to give tiny masses with small mass differences to the various light neutrino species. Radiative decay of the muon into electron is then possible but with an unobservable rate highly suppressed by the minuscule neutrino masses [1,2]. Searches for lepton flavor violating rare processes in high intensity experiments are thus important for new physics beyond the SM.

The most recent limit on the branching ratio $B(\mu \to e\gamma)$ is from the MEG experiment [3]

$$B(\mu \to e\gamma) \leq 4.2 \times 10^{-13}\ (90\%\,\text{C.L.}) \quad (\text{MEG}\,2016)\,, \tag{1}$$

and its projected improvement [4] is

$$B(\mu \to e\gamma) \sim 4 \times 10^{-14}\,. \tag{2}$$

Recent data from the T2K experiment [5] agrees well with the global analysis of neutrino oscillation data [6–9], suggesting that the normal neutrino mass hierarchy (NH) with a CP violating Dirac phase $\delta_{\text{CP}} \sim 3\pi/2$ is slightly preferred. The best fit result for the central values of the PMNS matrix elements in the normal neutrino mass hierarchy can be extracted from [6]

$$U^{\text{NH}}_{\text{PMNS}} = \begin{pmatrix} 0.8240 & 0.5471 & -0.02302 + 0.14536i \\ -0.40085 + 0.08042i & 0.63131 + 0.053399i & 0.65685 \\ 0.38169 + 0.09054i & -0.5437 + 0.06012i & 0.73952 \end{pmatrix}. \tag{3}$$

For the $\mu - e$ conversion in nuclei, the present experimental upper limits on the branching ratios were obtained by SINDRUM II experiment [10,11] for the targets titanium and gold,

$$B(\mu^- + \text{Ti} \to e^- + \text{Ti}) < 4.3 \times 10^{-12}\ (90\%\,\text{C.L.})\,, \tag{4}$$

$$B(\mu^- + \text{Au} \to e^- + \text{Au}) < 7 \times 10^{-13}\ (90\%\,\text{C.L.})\,. \tag{5}$$

Significant improvements are expected for $\mu - e$ conversion at future experiments like the Mu2e at Fermilab in US and the COMET at J-PARC in Japan. Projected sensitivities of $\mu - e$ conversion are [12,14,13,15,16]

$$B(\mu^- + \text{Al} \to e^- + \text{Al}) < 3 \times 10^{-17} \quad (\text{Mu2e, COMET})\,, \tag{6}$$

$$B(\mu^- + \text{Ti} \to e^- + \text{Ti}) < 10^{-18} \quad (\text{Mu2e II, PRISM})\,. \tag{7}$$

A positive signal of any of the above processes (or any process with charged lepton flavor violation (CLFV)) at the current or projected sensitivities of various high intensity experiments would be a clear indication of new physics as well, just like neutrino oscillations. Given the fact that no new physics has showed up yet at the high energy frontier of the Large Hadron Collider (LHC), it is not a surprise that many recent works have been focused on new physics implication of CLFV in the high intensity frontier. For a review on this topics and its possible connection with the muon anomaly, see [17] and references therein.

In a recent work [18], we updated a previous calculation [19] for the radiative process $\mu \to e\gamma$ in the mirror fermion model with electroweak scale non-sterile right-handed neutrinos [20] to an

extended version [21] where a horizontal A_4 symmetry was imposed in the lepton and scalar sectors. In this work we extend this previous analysis [18] to the $\mu - e$ conversion in nuclei, in particular for aluminum, gold and titanium.

The $\mu - e$ conversion had been studied extensively in many low-scale seesaw models beyond the SM [22–27]. One crucial difference is that the right-handed neutrinos are sterile in these models while in the mirror fermion model that we are studying they are non-sterile. This may lead to distinctive signatures like two jets or same sign dilepton in association with missing transverse energies and displaced vertices at the collider searches for the mirror quarks [28] or leptons [29].

This paper is organized as follows. In Sec. 2, we provide some highlights of the crucial features of the extended mirror fermion model. In Sec. 3, we briefly review the effective Lagrangian [30,31] for describing $\mu - e$ coherent conversion processes. In Sec. 4, we present the detailed calculation of $\mu - e$ conversion in the model. In Sec. 5, we derive a simple relation between the $\mu - e$ conversion rate and the radiative decay rate of $\mu \to e\gamma$ in the limit of zero momentum transfer and large mirror lepton masses. Numerical results are shown in Sec. 6. We summarize our results in Sec. 7. In Appendix A, we collect some useful formulas used in Secs. 4 and 5.

2. Mirror fermion model

In this section, we will provide some highlights for the original mirror fermion model [20] and its A_4 extension [21].

2.1. Motivation

The motivation of introducing mirror fermions in [20] was manifold. First of all, it is aesthetically satisfactory to have parity restoration at a higher energy scale while the maximal parity violating interaction (V−A interaction) in the SM emerges from spontaneous symmetry breaking. This is one of the main reasons for various left-right symmetric models in the literature [32–35]. Secondly, it is important to study non-perturbative effects in the SM by discretizing it on the lattice. However it is well known that putting chiral fermion on the lattice is plagued by fermion doubling – an unavoidable consequence of the no-go theorem proved by Nielsen and Ninomiya [36]. Sophisticated techniques like using Wilson fermion, Wilson–Ginsparg fermion, staggered fermion, or domain wall fermion *etc.*, which by violating at least one of the assumptions in the no-go theorem gets rid of the unwanted species, are often employed to handle this problem in practise. For new physics model builders, it is attractive to add mirror fermions to the SM which makes the theory becomes vector-like at a higher scale and hence one can avoid the fermion doubling problem if formulating on the lattice. Chiral gauge anomalies will then be cancelled automatically in this class of models. The third motivation is the electroweak scale non-sterile right-handed neutrinos introduced in [20]. For each generation, the right-handed neutrino is introduced together with a right-handed heavy charged fermion partner to form a SM $SU(2)$ doublet. Similarly a left-handed heavy mirror charged lepton will be introduced for each right-handed SM charged lepton. Majorana masses can then be given to these right-handed neutrinos via the vacuum expectation value (VEV) of a hypercharge $Y/2 = 1$ Higgs triplet with mass at the electroweak scale, rather than the grand unification scale in the usual scheme. Tiny Dirac masses can also be given via small VEVs of Higgs singlets with $Y = 0$. This is the electroweak scale see-saw mechanism in mirror fermion model which is testable at the LHC [28,29].

Table 1
The SM quantum numbers of the fermion and scalar sectors in the extended mirror fermion model together with their assignments under the horizontal A_4 symmetry. Subscript 'i' labels the generation. The electric charge Q equals $T_3 + Y/2$ in unit of e.

Fields	$(SU(3)\,,\, SU(2)\,,\, U(1)_Y\,;\, A_4)$
$l_{Li} = \begin{pmatrix} \nu_L \\ e_L \end{pmatrix}_i \;,\; l^M_{Ri} = \begin{pmatrix} \nu_R \\ e^M_R \end{pmatrix}_i$	$(1, 2, -\frac{1}{2}\,;\, 3)$
$e_{Ri} \;,\; e^M_{Li}$	$(1, 1, -1\,;\, 3)$
$q_{Li} = \begin{pmatrix} u_L \\ d_L \end{pmatrix}_i \;,\; q^M_{Ri} = \begin{pmatrix} u^M_R \\ d^M_R \end{pmatrix}_i$	$(3, 2, \frac{1}{6}\,;\, 3)$
$u_{Ri} \;,\; u^M_{Li}$	$(3, 1, \frac{2}{3}\,;\, 3)$
$d_{Ri} \;,\; d^M_{Li}$	$(3, 1, -\frac{1}{3}\,;\, 3)$
ϕ_{0S}	$(1, 1, 0\,;\, 1)$
$\vec{\phi}_S$	$(1, 1, 0\,;\, 3)$
$\Phi_2 \;,\; \Phi_{2M}$	$(1, 2, \frac{1}{2}\,;\, 1)$
ξ	$(1, 3, 0\,;\, 1)$
$\tilde{\chi}$	$(1, 3, 1\,;\, 1)$

The original model in [20] has been shown to be consistent with electroweak precision test data [37]. Later on, the original model was extended by including a mirror Higgs doublet [38] so as to accommodate the 125 GeV Higgs data from the LHC. In [21], the model with the mirror Higgs doublet [38] was further extended with a horizontal A_4 symmetry imposed in the lepton and Higgs sectors to address various issues of lepton mixings. We will briefly review these extensions of the original model in the next subsection.

2.2. *Particle content and its A_4 assignments*

The particle content of fermions and bosons of the model are shown in Table 1. The fields l^M_{Ri} and e^M_{Li} are the mirrors of the SM lepton doublet l_{Li} and singlet e_{Ri} respectively for the i-th generation. Similarly, q^M_{Ri}, u^M_{Li} and d^M_{Li} are the mirror partners of the SM quarks q_{Li}, u_{Ri} and d_{Ri} respectively. For the scalars, Φ_{2M} introduced in [38], is the mirror partner of SM Higgs doublet Φ_2; ξ and $\tilde{\chi}$ are the Georgi–Machacek (GM) triplets [39,40]; and ϕ_{0S} and $\vec{\phi}_S$ are gauge singlets introduced in [21]. The A_4 assignments of these particles are also listed in Table 1.

In the extended mirror fermion model of [38], the scalar sector consists of the two doublets Φ_2 and Φ_{2M}, and the GM triplets ξ and $\tilde{\chi}$. It has a total of 17 real scalar fields. A global symmetry $U(1)_{\rm SM} \times U(1)_{\rm MF}$ was also introduced in [38] such that Φ_2 only couples to the SM fermions and Φ_{2M} only couples to the mirror fermions. Thus there is no flavor changing neutral current interactions at tree level in the Yukawa couplings. Besides the three Nambu–Goldstone bosons, eaten by the longitudinal components of the $W^\pm$ and Z bosons after spontaneous symmetry breaking of $SU(2) \times U(1)_Y \longrightarrow U(1)_{\rm em}$, the remaining fourteen real fields are grouped into $5 + 3 + 3 + 1 + 1 + 1$ of a $SU(2)_D$, which is a residual symmetry of the breaking of the global custodial symmetry $SU(2)_L \times SU(2)_R \longrightarrow SU(2)_D$. The three singlets are the CP-even neutral Higgses, $\mathrm{Re}(\Phi^0_2)$, $\mathrm{Re}(\Phi^0_{2M})$ and $\frac{1}{3}(\sqrt{2}\mathrm{Re}(\tilde{\chi}^0) + \xi^0)$. While the states within the 5-plet and 3-plet are degenerate in masses, the three singlets can in general be mixed together. It was shown in [38] that the 125 GeV Higgs is an admixture of these three singlets, and these mixing effects

are essential to make the model consistent with the LHC data of the 125 GeV Higgs. All these scalars are A_4 singlets. While both ξ and $\tilde{\chi}$ are crucial to maintain the custodial symmetry at tree level, $\tilde{\chi}$ is responsible for providing the Majorana masses to the right-handed neutrinos mentioned earlier. Furthermore, the large contribution to the electroweak oblique parameters from the triplets was shown in [37] to be offset by the opposite contribution from the mirror fermions such that the model is safe against the electroweak precision data. To be specific, it was demonstrated in [37] that it is possible to find any combination of the parameter space, $m_Z \leq m_{\text{Higgses}}$, $m_{q^M} \leq 600$ GeV, $150 \leq m_{l^M} \leq 600$ GeV, $m_Z/2 \leq m_{\nu_R} \leq 600$ GeV, that can satisfy the electroweak precision data constraints on the oblique parameters within the 2σ region.

The weak singlet scalars ϕ_{0S} and $\vec{\phi}_S$ introduced in [21] are singlet and triplet under A_4 respectively. They are the only fields connecting the SM fermions and their mirror counterparts. Recall that the tetrahedron symmetry group A_4 has four irreducible representations $\mathbf{1}$, $\mathbf{1}'$, $\mathbf{1}''$, and $\mathbf{3}$. The multiplication rule that is relevant to us is[1]:

$$\begin{aligned}\mathbf{3}\times\mathbf{3} &= \mathbf{3_1}(23,31,12)+\mathbf{3_2}(32,13,21)\\ &+\mathbf{1}(11+22+33)+\mathbf{1}'(11+\omega^2 22+\omega 33)+\mathbf{1}''(11+\omega 22+\omega^2 33)\end{aligned} \tag{8}$$

where $\omega = e^{2\pi i/3}$. In the gauge eigenbasis (fields with superscript 0), one can write down the following A_4 invariant Yukawa couplings,[2]

$$\begin{aligned}-\mathcal{L}_{Yl} \supset\ & g_{0S}\phi_{0S}(\overline{l_L^0}l_R^{0M})_{\mathbf{1}} + g_{1S}\vec{\phi}_S\cdot(\overline{l_L^0}\times l_R^{0M})_{\mathbf{3_1}} + g_{2S}\vec{\phi}_S\cdot(\overline{l_L^0}\times l_R^{0M})_{\mathbf{3_2}} + \text{H.c.}\\ &+ g'_{0S}\phi_{0S}(\overline{e_R^0}e_L^{0M})_{\mathbf{1}} + g'_{1S}\vec{\phi}_S\cdot(\overline{e_R^0}\times e_L^{0M})_{\mathbf{3_1}} + g'_{2S}\vec{\phi}_S\cdot(\overline{e_R^0}\times e_L^{0M})_{\mathbf{3_2}} + \text{H.c.}\end{aligned} \tag{9}$$

Similar couplings can be written down for the quarks as well and we will describe them later.

As shown in [21], after the scalar singlets develop VEVs with $v_0 = \langle\phi_{0S}\rangle$ and $v_k = \langle\phi_{kS}\rangle$, one obtains the neutrino mass matrix from the first line of (9)

$$M_\nu^{\text{Dirac}} = \begin{pmatrix} g_{0S}v_0 & g_{1S}v_3 & g_{2S}v_2\\ g_{2S}v_3 & g_{0S}v_0 & g_{1S}v_1\\ g_{1S}v_2 & g_{2S}v_1 & g_{0S}v_0\end{pmatrix}. \tag{10}$$

Reality of the mass eigenvalues of M_ν^{Dirac} implies g_{0S} is real and $g_{2S} = g_{1S}^*$. Furthermore, if one assumes $v_i = v$, M_ν^{Dirac} reduces to

$$M_\nu^{\text{Dirac}} = \begin{pmatrix} g_{0S}v_0 & g_{1S}v & g_{1S}^*v\\ g_{1S}^*v & g_{0S}v_0 & g_{1S}v\\ g_{1S}v & g_{1S}^*v & g_{0S}v_0\end{pmatrix}. \tag{11}$$

The above form of M_ν^{Dirac} can be diagonalized by an unitary matrix U_ν, *i.e.* $U_\nu^\dagger M_\nu^{\text{Dirac}} U_\nu = M_\nu^{\text{Diag}}$ with [21]

$$U_\nu \equiv U_{\text{CW}}^\dagger = \frac{1}{\sqrt{3}}\begin{pmatrix}1 & 1 & 1\\ 1 & \omega^2 & \omega\\ 1 & \omega & \omega^2\end{pmatrix}, \tag{12}$$

[1] $\mathbf{3_1}$ is differ from $\mathbf{3_2}$ because A_4 is nonabelian.

[2] After spontaneous symmetry breaking the scalar singlets ϕ_{0S} and $\vec{\phi}_S$ might be mixing among each other as well as with other scalars in the model. We have assumed the quartic couplings responsible to these mixing effects are negligibly small so that ϕ_{0S} and $\vec{\phi}_S$ are the physical states.

where ω is the same as in the multiplication rules of A_4 given in (8). The matrix $U_{\rm CW}$ in (12) was first discussed by Cabibbo [41] and also by Wolfenstein [42] in the context of CP violation for three generations of neutrino oscillations.

On the other hand, the Majorana mass term for the right-handed neutrinos can be generated by the following A_4 invariant Lagrangian [21]

$$\mathcal{L}_M = g_M \left(l_R^{0M,T} \sigma_2 \right) (i\tau_2 \tilde{\chi})\, l_R^{0M} + \text{H.c.}\,. \tag{13}$$

When the neutral component of the A_4 singlet $\tilde{\chi}$ develops a VEV $\langle \chi_0 \rangle = v_M$, one obtains the Majorana mass matrix M_R [21]

$$M_R = g_M v_M \begin{pmatrix} 1 & 0 & 0 \\ 0 & 1 & 0 \\ 0 & 0 & 1 \end{pmatrix} . \tag{14}$$

The full neutrino mass matrix is given by

$$\mathcal{M}_\nu = \begin{pmatrix} 0 & M_\nu^{\rm Dirac} \\ \left(M_\nu^{\rm Dirac}\right)^{\rm T} & M_R \end{pmatrix} , \tag{15}$$

with $M_\nu^{\rm Dirac}$ and M_R given by (11) and (14) respectively. The light neutrino mass matrix is then

$$m_\nu \sim -M_\nu^{\rm Dirac} M_R^{-1} \left(M_\nu^{\rm Dirac}\right)^{\rm T} = -\frac{1}{g_M v_M} M_\nu^{\rm Dirac} \left(M_\nu^{\rm Dirac}\right)^{\rm T} , \tag{16}$$

where we have used the fact that M_R in (14) is proportional to the unit matrix. We note that an unitary matrix U_ν that diagonalizes the Dirac mass matrix $M_\nu^{\rm Dirac}$ in general won't diagonalize the light neutrino mass matrix m_ν. However, with $M_\nu^{\rm Dirac}$ given by (11) in the model, one can check readily that the light neutrino mass matrix m_ν in (16) can be diagonalized by U_ν given by (12) as well.

Note also that the true light neutrino masses should be obtained by block-diagonalization [43–46] of the full neutrino mass matrix $\mathcal{M}_\nu$ in (15). The m_ν given by (16) can only be regarded as an effective light neutrino mass matrix obtained by integrating out the heavy degrees of freedom represented by the heavy Majorana fermions with mass of order M_R. Thus it may receive subleading corrections upon block-diagonalization of $\mathcal{M}_\nu$. For the purposes of this work, since $M_R \gg \langle \phi_{0S} \rangle, \langle \phi_{iS} \rangle$, it is sufficient to consider the effective light neutrino mass matrix. The PMNS neutrino mixing matrix is then given by $U_{\rm PMNS} = U_\nu^\dagger U_L^l$ where U_L^l is the unitary matrix that diagonalizes the charged lepton mass matrix squared. A phenomenological approach was proposed in [21] to parameterize U_L^l as deviating from unity in the form of a Wolfenstein-like unitary matrix. Using the experimental input for the matrix elements of $U_{\rm PMNS}$, the allowed ranges for the Wolfenstein parameters in U_L^l can be deduced [21].

We note that this discrete A_4 symmetry does not forbid the quartic couplings of the Higgs singlets with the doublets and triplets. After symmetry breaking, these would lead to additional scalar mixings not considered before in [38] which can give contributions to the invisible width for the 125 GeV Higgs. As shown in [38], the mixings between the neutral components of the two Higgs doublets and the GM triplets are tightly constrained already by the LHC data for the signal strengths of the 125 GeV Higgs. Including the singlets in the mixings is beyond the scope of this work. However they are expected to be tightly constrained as well. We will assume these additional scalar mixings are small enough in order to circumvent the LHC data on the Higgs invisible width and signal strengths.

In recent years, advocating A_4 symmetry in the lepton sector was mainly due to Ma [47]. For an elementary introduction of the A_4 discrete group, see for example [48].

2.3. Mixings

Let $U^l_{L,R}$ and $U^{l^M}_{R,L}$ be the unitary matrices relating the gauge eigenstates and the mass eigenstates (fields without superscripts 0) of the SM and mirror fermions defined as

$$l^0_L = U^l_L l_L \ , \ e^0_R = U^l_R e_R \ , \ l^{M,0}_R = U^{l^M}_R l^M_R \ , \ e^{M,0}_L = U^{l^M}_L e^M_L \ . \tag{17}$$

Following [18], we express the Yukawa couplings in (9) as follows

$$\mathcal{L}_{Yl} \supset -\sum_{k=0}^{3}\sum_{i,m=1}^{3}\left(\bar{l}_{Li}\,\mathcal{U}^{L\,k}_{im}\,l^M_{Rm} + \bar{e}_{Ri}\,\mathcal{U}^{R\,k}_{im}\,e^M_{Lm}\right)\phi_{kS} + \text{H.c.} \tag{18}$$

The coupling coefficients $\mathcal{U}^{L\,k}_{im}$ and $\mathcal{U}^{R\,k}_{im}$ are given by

$$\begin{aligned}\mathcal{U}^{L\,k}_{im} &\equiv \left(U^{\dagger}_{\text{PMNS}}\cdot M^k\cdot U^M_{\text{PMNS}}\right)_{im} \ , \\ &= \sum_{j,n=1}^{3}\left(U^{\dagger}_{\text{PMNS}}\right)_{ij} M^k_{jn}\left(U^M_{\text{PMNS}}\right)_{nm} \ ,\end{aligned} \tag{19}$$

and

$$\begin{aligned}\mathcal{U}^{R\,k}_{im} &\equiv \left(U'^{\dagger}_{\text{PMNS}}\cdot M'^k\cdot U'^M_{\text{PMNS}}\right)_{im} \ , \\ &= \sum_{j,n=1}^{3}\left(U'^{\dagger}_{\text{PMNS}}\right)_{ij} M'^k_{jn}\left(U'^M_{\text{PMNS}}\right)_{nm} \ ,\end{aligned} \tag{20}$$

where the matrix elements for the four auxiliary matrices $M^k (k = 0, 1, 2, 3)$ are listed in Table 2, and M'^k_{jn} can be obtained from M^k_{jn} with the following substitutions for the Yukawa couplings $g_{0S} \to g'_{0S}$ and $g_{1S} \to g'_{1S}$; U_{PMNS} is the usual neutrino mixing matrix defined as

$$U_{\text{PMNS}} = U^{\dagger}_{\nu} U^l_L \, , \tag{21}$$

and its mirror and right-handed counter-parts U^M_{PMNS}, U'_{PMNS} and U'^M_{PMNS} are defined analogously as

$$U^M_{\text{PMNS}} = U^{\dagger}_{\nu} U^{l^M}_R \, , \tag{22}$$

$$U'_{\text{PMNS}} = U^{\dagger}_{\nu} U^l_R \, , \tag{23}$$

and

$$U'^M_{\text{PMNS}} = U^{\dagger}_{\nu} U^{l^M}_L \ . \tag{24}$$

Table 2
Matrix elements for the four auxiliary $M^k (k = 0, 1, 2, 3)$ where $\omega \equiv \exp(i2\pi/3)$ and g_{0S} and g_{1S} are complex Yukawa couplings. M'^k can be obtained from M^k with the following substitutions $g_{0S} \to g'_{0S}$ and $g_{1S} \to g'_{1S}$.

M^k_{jn}	Value
$M^0_{12}, M^0_{13}, M^0_{21}, M^0_{23}, M^0_{31}, M^0_{32}$	0
$M^0_{11}, M^0_{22}, M^0_{33}$	g_{0S}
$M^1_{11}, M^2_{11}, M^3_{11}; M^1_{23}, M^1_{32}$	$\frac{2}{3}\mathrm{Re}\,(g_{1S})$
$M^1_{22}, M^2_{22}, M^3_{22}; M^1_{13}, M^1_{31}$	$\frac{2}{3}\mathrm{Re}\,(\omega^* g_{1S})$
$M^1_{33}, M^2_{33}, M^3_{33}; M^1_{12}, M^1_{21}$	$\frac{2}{3}\mathrm{Re}\,(\omega g_{1S})$
M^2_{12}, M^3_{21}	$\frac{1}{3}\left(g_{1S} + \omega g^*_{1S}\right)$
M^3_{12}, M^2_{21}	$\frac{1}{3}\left(g^*_{1S} + \omega^* g_{1S}\right)$
M^2_{13}, M^3_{31}	$\frac{1}{3}\left(g_{1S} + \omega^* g^*_{1S}\right)$
M^3_{13}, M^2_{31}	$\frac{1}{3}\left(g^*_{1S} + \omega g_{1S}\right)$
M^2_{23}, M^3_{32}	$\frac{2\omega^*}{3}\mathrm{Re}\,(g_{1S})$
M^3_{23}, M^2_{32}	$\frac{2\omega}{3}\mathrm{Re}\,(g_{1S})$

3. Effective Lagrangian for $\mu - e$ conversion

Effective Lagrangian is a powerful technique to analyse low energy processes like $\mu \to e$ conversion in nuclei since the momentum transfer q^2 is typically of the order $\mathcal{O}(m_\mu^2) \ll m_N^2$ for nucleus N. The most general CLFV effective Lagrangian which contributes to the $\mu - e$ conversion in nuclei has been studied by various groups [30,31,49]. At the scale Λ where the heavy particles (including particles beyond the SM as well as the heavy top, bottom and charm quarks) being integrated out, the relevant terms for the model we are studying are

$$\begin{aligned}\mathcal{L}_{\rm eff} = -\frac{1}{\Lambda^2}\Bigg[&\left(C_{DR} m_\mu \overline{e}\sigma^{\alpha\beta} P_L \mu + C_{DL} m_\mu \overline{e}\sigma^{\alpha\beta} P_R \mu\right) F_{\alpha\beta} \\ &+ \sum_{q=u,d,s} \left(C^{(q)}_{VR}\overline{e}\gamma^\alpha P_R\mu + C^{(q)}_{VL}\overline{e}\gamma^\alpha P_L\mu\right)\overline{q}\gamma_\alpha q \\ &+ \sum_{q=u,d,s} m_\mu m_q G_F \left(C^{(q)}_{SR}\overline{e}P_R\mu + C^{(q)}_{SL}\overline{e}P_L\mu\right)\overline{q}q \\ &+ m_\mu \left(C_{GQR} G_F \overline{e}P_L\mu + C_{GQL} G_F \overline{e}P_R\mu\right)\frac{\beta_L}{2g_s^3} G^{a\alpha\beta} G^a_{\alpha\beta} + \mathrm{H.c.}\Bigg].\end{aligned} \tag{25}$$

Here G_F, m_μ and m_q are the Fermi constant, muon and quark masses respectively; $P_{L,R} = (1 \mp \gamma_5)/2$, $\sigma_{\mu\nu} = i\left[\gamma_\mu, \gamma_\nu\right]/2$; $F_{\alpha\beta}$ is the electromagnetic field strength; $G^a_{\alpha\beta}$ is the QCD gluon field strength with β_L its beta function $\beta_{\rm QCD} \equiv (g_s^3/16\pi^2)(11 - 2N_F/3)$ of three light flavors ($N_F = 3$) and g_s is the strong coupling constant; finally, $C_{D(L,R)}$, $C^{(q)}_{V(L,R)}$, $C^{(q)}_{S(L,R)}$ and $C_{GQ(L,R)}$ are dimensionless coupling constants depending on specific LFV model. In (25) the following quark bilinears $\overline{q}\gamma_5 q$, $\overline{q}\gamma_\mu\gamma_5 q$ and $\overline{q}\sigma_{\mu\nu}q$ are not included since they do not contribute for coherent conversion processes in which the initial and final states of the nucleus are the same.

To determine the conversion rate, the above effective Lagrangian (25) is needed to scale down to the nuclear scale where the hadronic matrix elements $\langle N|\overline{q}q|N\rangle$, $\langle N|\overline{q}\gamma_\mu q|N\rangle$,

$\langle N|F^{\alpha\beta}F_{\alpha\beta}|N\rangle$ and $\langle N|G^{a\alpha\beta}G^{a}_{\alpha\beta}|N\rangle$ are evaluated. In addition, the muon and electron wave functions may be significantly deviating from plane wave due to distortion by the coulomb potential of the nuclei. For high Z nuclei, relativistic corrections to their wave functions are important as well. The formula for the conversion rate is given by [31,49]

$$\begin{aligned}\Gamma_{\rm conv} = \frac{m_\mu^5}{4\Lambda^4}\Bigg(&\Big|C_{DR}D + 4\tilde{C}^{(p)}_{VR}V^{(p)} \\ &+ 4\tilde{C}^{(n)}_{VR}V^{(n)} + 4G_F m_\mu\left(m_p\tilde{C}^{(p)}_{SR}S^{(p)} + m_n\tilde{C}^{(n)}_{SR}S^{(n)}\right)\Big|^2 \\ &+ \Big|C_{DL}D + 4\tilde{C}^{(p)}_{VL}V^{(p)} + 4\tilde{C}^{(n)}_{VL}V^{(n)} \\ &+ 4G_F m_\mu\left(m_p\tilde{C}^{(p)}_{SL}S^{(p)} + m_n\tilde{C}^{(n)}_{SL}S^{(n)}\right)\Big|^2\Bigg)\,.\end{aligned} \tag{26}$$

In (26) the coupling constants $\tilde{C}^{(p,n)}_{V(R,L)}$ are defined as [49]

$$\begin{aligned}\tilde{C}^{(p)}_{VR} &= \sum_{q=u,d,s} C^{(q)}_{VR} f^{(q)}_{Vp}\,, \\ \tilde{C}^{(n)}_{VR} &= \sum_{q=u,d,s} C^{(q)}_{VR} f^{(q)}_{Vn}\,, \\ \tilde{C}^{(p)}_{VL} &= \sum_{q=u,d,s} C^{(q)}_{VL} f^{(q)}_{Vp}\,, \\ \tilde{C}^{(n)}_{VL} &= \sum_{q=u,d,s} C^{(q)}_{VL} f^{(q)}_{Vn}\,,\end{aligned} \tag{27}$$

where $f^{(q)}_{Vp}$ and $f^{(q)}_{Vn}$ are the known nucleon vector form factors

$$\begin{aligned}&f^{(u)}_{Vp} = 2, \quad f^{(d)}_{Vp} = 1, \quad f^{(s)}_{Vp} = 0\,, \\ &f^{(u)}_{Vn} = 1, \quad f^{(d)}_{Vn} = 2, \quad f^{(s)}_{Vn} = 0\,;\end{aligned} \tag{28}$$

and

$$\begin{aligned}\tilde{C}^{(p)}_{SR} &= \sum_{q=u,d,s} C^{(q)}_{SR} f^{(q)}_{Sp} + C_{GQR}\left(1 - \sum_{q=u,d,s} f^{(q)}_{Sp}\right)\,, \\ \tilde{C}^{(n)}_{SR} &= \sum_{q=u,d,s} C^{(q)}_{SR} f^{(q)}_{Sn} + C_{GQR}\left(1 - \sum_{q=u,d,s} f^{(q)}_{Sn}\right)\,, \\ \tilde{C}^{(p)}_{SL} &= \sum_{q=u,d,s} C^{(q)}_{SL} f^{(q)}_{Sp} + C_{GQL}\left(1 - \sum_{q=u,d,s} f^{(q)}_{Sp}\right)\,, \\ \tilde{C}^{(n)}_{SL} &= \sum_{q=u,d,s} C^{(q)}_{SL} f^{(q)}_{Sn} + C_{GQL}\left(1 - \sum_{q=u,d,s} f^{(q)}_{Sn}\right)\,,\end{aligned} \tag{29}$$

Table 3
Values of the dimensionless overlap integrals for aluminum, titanium and gold, evaluated under the assumption that the proton and neutron distributions within each nuclei are the same [31].

Nucleus	D	$V^{(p)}$	$V^{(n)}$	$S^{(p)}$	$S^{(n)}$
$^{27}_{13}$Al	0.0362	0.0161	0.0173	0.0155	0.0167
$^{48}_{22}$Ti	0.0864	0.0396	0.0468	0.0368	0.0435
$^{197}_{79}$Au	0.189	0.0974	0.146	0.0614	0.0918

where $f_{Sp}^{(q)}$ and $f_{Sn}^{(q)}$ are the scalar nucleon form factors, which can be expressed in terms of nucleon matrix elements and ratios of quarks masses according to [50]:

$$\begin{aligned}
f_{Sp}^{(u)} &= \frac{m_u}{m_u+m_d}\frac{\sigma_{\pi N}}{m_p}(1+\xi)\ ,\\
f_{Sp}^{(d)} &= \frac{m_d}{m_u+m_d}\frac{\sigma_{\pi N}}{m_p}(1-\xi)\ ,\\
f_{Sp}^{(s)} &= \frac{m_s}{m_u+m_d}\frac{\sigma_{\pi N}}{m_p}y\ ,\\
f_{Sn}^{(u)} &= \frac{m_u}{m_u+m_d}\frac{\sigma_{\pi N}}{m_p}(1-\xi)\ ,\\
f_{Sn}^{(d)} &= \frac{m_d}{m_u+m_d}\frac{\sigma_{\pi N}}{m_p}(1+\xi)\ ,\\
f_{Sn}^{(s)} &= \frac{m_s}{m_u+m_d}\frac{\sigma_{\pi N}}{m_p}y\ ,
\end{aligned} \tag{30}$$

where

$$\begin{aligned}
\sigma_{\pi N} &= \frac{m_u+m_d}{2}\langle N|\bar{u}u+\bar{d}d|N\rangle\ ,\\
\xi &= \frac{\langle p|\bar{u}u-\bar{d}d|p\rangle}{\langle p|\bar{u}u+\bar{d}d|p\rangle}\ ,\\
y &= 2\frac{\langle p|\bar{s}s|p\rangle}{\langle p|\bar{u}u+\bar{d}d|p\rangle}\ .
\end{aligned} \tag{31}$$

To evaluate the nucleon matrix elements in (31), one can adopt a recent updated analysis given in [51]. Choosing the second row of Table I of [51], corresponding to an input value of $\sigma_s = m_s\langle p|\bar{s}s|p\rangle = 50$ MeV, we have the central values

$$\sigma_{\pi N} = 39.8\ \text{MeV}\ ,\ \xi = 0.18\ ,\ y = 0.09\ , \tag{32}$$

where the current quark masses have been taken to be [51,52]

$$m_u = 2.5^{+0.6}_{-0.8}\,\text{MeV}\ ,\ \ m_d = 5.0^{+0.7}_{-0.9}\,\text{MeV}\ ,\ \ m_s = 100^{+30}_{-20}\,\text{MeV}\ , \tag{33}$$

normalized at the scale $\mu = 2$ GeV.

The dimensionless quantities D, $V^{(p,n)}$ and $S^{(p,n)}$ in (26) are the overlap integrals of the relativistic wave functions of muon and electron in the electric field of the nucleus weighted by appropriate combinations of proton and neutron densities [31]. Their values for the three nuclei aluminum, titanium and gold are listed in Table 3 for reference.

Table 4
Standard model values of the capture rates for aluminum, titanium and gold in unit of 10^6 s^{-1} taken from Ref. [53].

Nucleus	Γ_{capt} (10^6 s^{-1})
$^{27}_{13}$Al	0.7054
$^{48}_{22}$Ti	2.59
$^{197}_{79}$Au	13.07

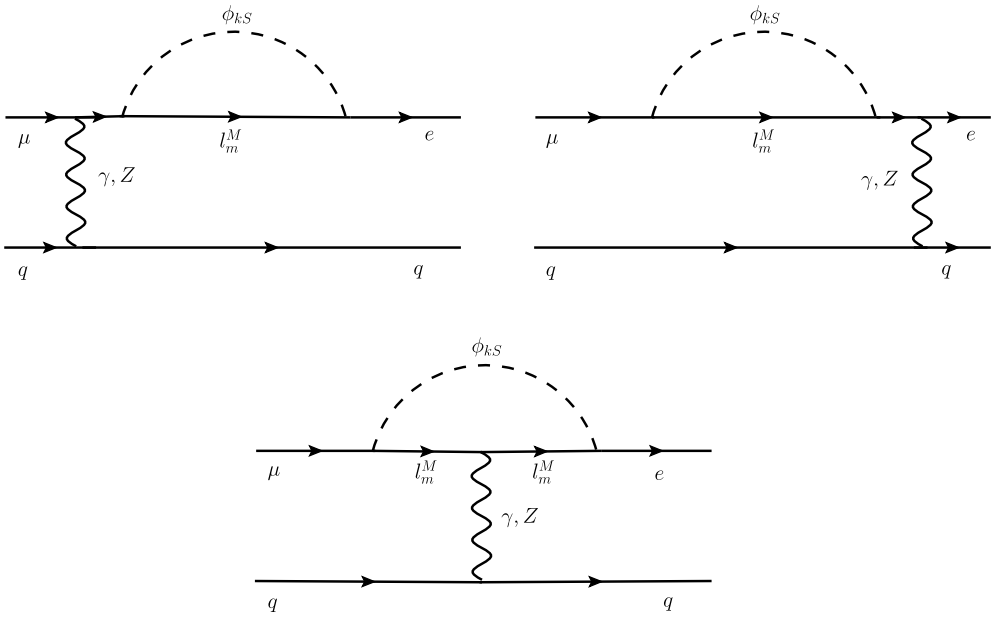

Fig. 1. One-loop induced Feynman diagrams from photon and Z boson exchanges for $\mu - e$ conversion in electroweak-scale ν_R model.

The $\mu - e$ conversion branching ratio is defined as

$$B_{\mu N \to eN}(Z, A) \equiv \frac{\Gamma_{\text{conv}}}{\Gamma_{\text{capt}}}\,, \tag{34}$$

where Γ_{conv} is given by (26) and Γ_{capt} is the standard model muon capture rate. The SM capture rates for aluminum, titanium and gold have been determined experimentally [53] and they are listed in Table 4 for convenience.

4. Mirror Fermion model calculation

4.1. Photon contributions and the monopole and dipole form factors

In this subsection we will focus on the contributions from the photon exchange Feynman diagrams as shown in Fig. 1. We also compute the contributions from the Z-exchange, Higgs

exchange as well as box diagrams but we will demonstrate in Sec. 6 they are numerically insignificant in the model. We note that the right-handed neutrinos do not contribute to $\mu - e$ conversion since there is neither $l_i - \nu_{Rj} -$ charged Higgs nor $l_i - \nu_{Rj} - W$ boson vertex in the model [38].

The invariant amplitude for $\mu^-(p) \to e^-(p')\gamma^*(q)$ with an off-shell photon can be parametrized as

$$i\mathcal{M}_\gamma = -e\overline{u}_e(p')i\Gamma^\mu_\gamma(q)u_\mu(p)A^*_\mu(q) \tag{35}$$

where $\Gamma^\mu_\gamma(q)$ has the following Lorentz and gauge invariant decomposition

$$\Gamma^\mu_\gamma(q) = \Big(f_{E0}(q^2) + \gamma_5 f_{M0}(q^2)\Big)\left(\gamma^\mu - \frac{q_\mu \not{q}}{q^2}\right) + \Big(f_{M1}(q^2) + \gamma_5 f_{E1}(q^2)\Big)\frac{i\sigma^{\mu\nu}q_\nu}{m_\mu}\,. \tag{36}$$

The monopole form factors f_{E0}, f_{M0} and the dipole form factors f_{M1}, f_{E1} can be obtained by generalizing our previous on-shell calculation of $\mu \to e\gamma$ in the same model [18] to the case of off-shell photon γ^*. From the Feynman diagrams of Fig. 1, we obtain the following expressions

$$\begin{aligned} f_{E0,M0}(q^2) = +\frac{1}{32\pi^2}\sum_{k,m}\int_0^1 dx\int_0^{1-x} dy\Bigg\{ & \frac{xyq^2}{M_m^2\Delta_{km}(q^2)}\left(\mathcal{U}^{Lk}_{1m}\left(\mathcal{U}^{Lk}_{2m}\right)^* \pm \mathcal{U}^{Rk}_{1m}\left(\mathcal{U}^{Rk}_{2m}\right)^*\right) \\ & - \Bigg[\log\left(\frac{\Delta_{km}(q^2)}{\Delta_{km}(0)}\right) - \left(M_m^2 \pm (1-x-y)^2 m_\mu m_e\right)\left(\frac{1}{M_m^2}\right) \\ & \times\left(\Delta^{-1}_{km}(q^2) - \Delta^{-1}_{km}(0)\right)\Bigg] \\ & \times\left(\mathcal{U}^{Lk}_{1m}\left(\mathcal{U}^{Lk}_{2m}\right)^* \pm \mathcal{U}^{Rk}_{1m}\left(\mathcal{U}^{Rk}_{2m}\right)^*\right) \\ & + (1-x-y)(m_\mu \pm m_e)\left(\frac{1}{M_m}\right)\left(\Delta^{-1}_{km}(q^2) - \Delta^{-1}_{km}(0)\right) \\ & \times\left(\mathcal{U}^{Lk}_{1m}\left(\mathcal{U}^{Rk}_{2m}\right)^* \pm \mathcal{U}^{Rk}_{1m}\left(\mathcal{U}^{Lk}_{2m}\right)^*\right)\Bigg\} \end{aligned} \tag{37}$$

for the monopole form factors, and

$$\begin{aligned} f_{M1,E1}(q^2) = -\frac{m_\mu}{32\pi^2}\sum_{k,m}\int_0^1 dx\int_0^{1-x} dy\,\frac{1}{M_m^2\Delta_{km}(q^2)} & \\ \times\Bigg\{(1-x-y)\left(ym_\mu \pm xm_e\right)\left(\mathcal{U}^{Lk}_{1m}\left(\mathcal{U}^{Lk}_{2m}\right)^* \pm \mathcal{U}^{Rk}_{1m}\left(\mathcal{U}^{Rk}_{2m}\right)^*\right) & \\ + (x+y)M_m\left(\mathcal{U}^{Lk}_{1m}\left(\mathcal{U}^{Rk}_{2m}\right)^* \pm \mathcal{U}^{Rk}_{1m}\left(\mathcal{U}^{Lk}_{2m}\right)^*\right)\Bigg\} & \end{aligned} \tag{38}$$

for the dipole form factors. Here, we have defined

$$\Delta_{km}(q^2) = (x+y) + (1-x-y)(m_k^2 - xm_e^2 - ym_\mu^2)\frac{1}{M_m^2} - xy\frac{q^2}{M_m^2} - i0^+\,, \tag{39}$$

where m_k denotes the mass of scalar singlet ϕ_{kS} for $k = 0, 1, 2, 3$ and M_m the mass of mirror lepton l^M_m for $m = 1, 2, 3$.

At $q^2 = 0$, we have $f_{E0,M0}(0) = 0$ as one would expect. Thus the following reduced monopole form factors $\tilde{f}_{E0,M0}$ with an explicit factor of q^2 extracted from $f_{E0,M0}$ are often defined in the literature,

$$f_{E0,M0}(q^2) = \frac{q^2}{m_\mu^2}\tilde{f}_{E0,M0}(q^2)\,. \tag{40}$$

For small q^2, one can set $\tilde{f}_{E0,M0}(q^2) \approx \tilde{f}_{E0,M0}(0)$ with

$$\begin{aligned}\tilde{f}_{E0,M0}(0) = \frac{m_\mu^2}{32\pi^2}\sum_{k,m}\int_0^1 dx\int_0^{1-x} dy\,\frac{xy}{\left(M_m^2\Delta_{km}(0)\right)^2}\Big\{&\left(\mathcal{U}_{1m}^{L\,k}\left(\mathcal{U}_{2m}^{L\,k}\right)^* \pm \mathcal{U}_{1m}^{R\,k}\left(\mathcal{U}_{2m}^{R\,k}\right)^*\right)\\ &\times\left(2M_m^2\Delta_{km}(0) + M_m^2 \pm (1-x-y)^2 m_\mu m_e\right)\\ &+\left(\mathcal{U}_{1m}^{L\,k}\left(\mathcal{U}_{2m}^{R\,k}\right)^* \pm \mathcal{U}_{1m}^{R\,k}\left(\mathcal{U}_{2m}^{L\,k}\right)^*\right)(1-x-y)(m_\mu \pm m_e)M_m\Big\}.\end{aligned} \tag{41}$$

The explicit factor of q^2 in (40) will cancel the $1/q^2$ of the photon propagator in Fig. 1. This leads to four-fermion vector–vector interaction and hence the reduced monopole form factors will contribute to the effective coupling $C^{(q)}_{V(R,L)}$ in the effective Lagrangian of (25) in Sec. 3. We will discuss more about these four-fermion interactions in the next subsection.

At $q^2 = 0$, the contributions from the magnetic and electric dipole terms of (36) to the amplitude $\mathcal{M}_\gamma$ in (35) can be reproduced by the following effective Lagrangian

$$\mathcal{L}_{\gamma,\text{eff}} = \frac{e}{2m_\mu}\overline{e}\sigma^{\alpha\beta}\left(f_{M1}(0) + \gamma_5 f_{E1}(0)\right)\mu F_{\alpha\beta} + \text{H.c.}\,, \tag{42}$$

where $F_{\alpha\beta}$ is the electromagnetic field strength. Comparing (42) with the first line of the general form of the Lagrangian for $\mu - e$ conversion given in (25) in Sec. 3, one can deduce the dimensionless effective couplings $C_{DR,DL}$ as linear combinations of the static limit of the dipole form factors f_{E1} and f_{M1},

$$\frac{C_{DR,DL}}{\Lambda^2} = \frac{e}{2m_\mu^2}\left(\pm f_{E1}(0) - f_{M1}(0)\right)\,. \tag{43}$$

4.2. Four-Fermion coupling coefficients

4.2.1. Photon exchange

The amplitude for $\mu(p)q(k) \to e(p')q(k')$ from the monopole form factors of the photon exchange in Fig. 1 can be obtained as

$$\mathcal{M}_\gamma = -e^2 Q_q\overline{u_e}(p')\left(f_{E0}(q^2) + f_{M0}(q^2)\gamma_5\right)\left(\gamma_\mu - \frac{q_\mu \not{q}}{q^2}\right)u_\mu(p)\frac{1}{q^2}\overline{u_q}(k')\gamma^\mu u_q(k)\,, \tag{44}$$

where $q = p - p' = k' - k$, and f_{E0}, f_{M0} are given in (37). The q_μ term in (44) can be dropped due to quark current conservation. As mentioned earlier, the $1/q^2$ of the photon propagator will be cancelled from a factor of q^2 in $f_{E0,M0}$. Thus in terms of the reduced form factors $\tilde{f}_{E0,M0}$ of (40), the amplitude $\mathcal{M}_\gamma$ can be rewritten as

$$\mathcal{M}_\gamma = -\frac{e^2 Q_q}{m_\mu^2}\left[\left(\tilde{f}_{E0}-\tilde{f}_{M0}\right)\overline{u_{Le}}(p')\gamma_\mu u_{L\mu}(p)+\left(\tilde{f}_{E0}+\tilde{f}_{M0}\right)\overline{u_{Re}}(p')\gamma_\mu u_{R\mu}(p)\right]$$
$$\times\left[\overline{u_{Lq}}(k')\gamma^\mu u_{Lq}(k)+\overline{u_{Rq}}(k')\gamma^\mu u_{Rq}(k)\right], \tag{45}$$

where $\tilde{f}_{E0,M0}$ are defined in (41) for small q^2. At $q^2=0$, this amplitude can be reproduced by the following Fermi interaction

$$\mathcal{L}'_{\gamma,\text{eff}} = -\frac{e^2 Q_q}{m_\mu^2}\left[\left(\tilde{f}_{E0}(0)-\tilde{f}_{M0}(0)\right)\overline{e_L}\gamma_\mu\mu_L+\left(\tilde{f}_{E0}(0)+\tilde{f}_{M0}(0)\right)\overline{e_R}\gamma_\mu\mu_R\right]$$
$$\cdot\left[\overline{q}\gamma^\mu q\right]. \tag{46}$$

By matching (46) with the second line of the general form of the Lagrangian for $\mu-e$ conversion given in (25) in Sec. 3, we deduce the following relations for the dimensionless effective couplings $C^{(q)\gamma}_{V(L,R)}$

$$\frac{C^{(q)\gamma}_{V(L,R)}(0)}{\Lambda^2} = \frac{e^2 Q_q}{m_\mu^2}\left(\tilde{f}_{E0}(0)\mp\tilde{f}_{M0}(0)\right). \tag{47}$$

Note that we have the relation $C^{(u)\gamma}_{V(L,R)} = -2C^{(d)\gamma}_{V(L,R)}$. This implies the vector effective couplings $\tilde{C}^{(n)\gamma}_{V(L,R)}$ for the neutron from the photon exchange are vanishing. This is expected since neutron carries no electric charge.

4.2.2. Z boson exchange

For the Z boson contributions from Fig. (1), in the limit of $|q^2| \ll m_Z^2$, we obtain the following amplitude

$$\mathcal{M}_Z \approx \frac{G_F}{\sqrt{2}}\left[f_L^Z(q^2)\,\overline{u_{Le}}(p')\gamma_\mu u_{L\mu}(p)+f_R^Z(q^2)\,\overline{u_{Re}}(p')\gamma_\mu u_{R\mu}(p)\right]$$
$$\times\left[\overline{u_q}(k')\left(C_V^q\gamma^\mu+C_A^q\gamma^\mu\gamma^5\right)u_q(k)\right], \tag{48}$$

where the $f^Z_{L,R}(q^2)$ are the form factors given by

$$f_L^Z(q^2) = \frac{1}{2\pi^2}\sum_{k,m}\int_0^1 dx\int_0^{1-x} dy$$
$$\left\{\left[\log\left(\frac{\Delta_{km}(q^2)}{\Delta_{km}(0)}\right)C_L^l-\left(\Delta_{km}^{-1}(q^2)-\Delta_{km}^{-1}(0)\right)C_R^l\right]\mathcal{U}_{1m}^{Lk}\left(\mathcal{U}_{2m}^{Lk}\right)^*\right.$$
$$-m_\mu m_e\frac{1}{M_m^2}(1-x-y)^2\left(\Delta_{km}^{-1}(q^2)-\Delta_{km}^{-1}(0)\right)C_R^l\mathcal{U}_{1m}^{Rk}\left(\mathcal{U}_{2m}^{Rk}\right)^*$$
$$-\frac{1}{M_m}(1-x-y)\left(\Delta_{km}^{-1}(q^2)-\Delta_{km}^{-1}(0)\right)C_R^l\left(m_\mu\mathcal{U}_{1m}^{Lk}\left(\mathcal{U}_{2m}^{Rk}\right)^*\right.$$
$$\left.\left.+m_e\mathcal{U}_{1m}^{Rk}\left(\mathcal{U}_{2m}^{Lk}\right)^*\right)-\frac{xyq^2}{M_m^2\Delta_{km}(q^2)}C_L^l\mathcal{U}_{1m}^{Lk}\left(\mathcal{U}_{2m}^{Lk}\right)^*\right\}$$
$$+\frac{(C_L^l-C_R^l)}{16\pi^2(m_\mu^2-m_e^2)}\sum_{k,m}\int_0^1 dx\log\left(\frac{\Delta^e_{km}(x)}{\Delta^\mu_{km}(x)}\right)\left\{\frac{M_m^2}{1-x}\mathcal{U}_{1m}^{Lk}\left(\mathcal{U}_{2m}^{Lk}\right)^*\right.$$

$$+ m_\mu m_e (1-x)\mathcal{U}^{R\,k}_{1m}\left(\mathcal{U}^{R\,k}_{2m}\right)^* + M_m\left(m_\mu \mathcal{U}^{L\,k}_{1m}\left(\mathcal{U}^{R\,k}_{2m}\right)^* + m_e \mathcal{U}^{R\,k}_{1m}\left(\mathcal{U}^{L\,k}_{2m}\right)^*\right)\Bigg\}, \tag{49}$$

and $f^Z_R(q^2)$ can be obtained from $f^Z_L(q^2)$ in (49) with $L \leftrightarrow R$ for all the quantities with L, R subscripts or superscripts. Here $C^f_L = T^3(f) - Q_f \sin^2\theta_W$ and $C^f_R = -Q_f \sin^2\theta_W$ are the chiral couplings of fermion f with the Z boson. We have used the fact that for muon, electron and mirror charged leptons they all have the same $C^l_{L,R}$. $\Delta_{km}(q^2)$ in (49) is given by (39) and $\Delta^{\mu,e}_{km}(x)$ is given by

$$\Delta^{\mu,e}_{km}(x) = x + (1-x)\frac{m^2_k}{M^2_m} - x(1-x)\frac{m^2_{\mu,e}}{M^2_m}\,. \tag{50}$$

In the derivation of (49) for $f^Z_L(q^2)$ (and the analogous $f^Z_R(q^2)$), we have dropped terms proportional to q_μ and $i\sigma_{\mu\nu}q^\nu$ from the Z-vertex diagram. The $q_\mu = (k'-k)_\mu$ term when multiplying the quark current $\overline{u}(k')\gamma^\mu(C^q_V + \gamma^5 C^q_A)u(k)$ in (48) will give zero in the vector part by using the free quark equation of motion, while for the axial vector part it will produce term proportional to the light quark mass. The $i\sigma_{\mu\nu}q^\nu$ term will give rise to dimension 7 4-fermion operators from (48) with one derivative in the position space. Both contributions will be suppressed by $\mathcal{O}(m_{\mu,q}/M)$ where M is the mass of heavy mirror fermion running inside the loop as compared with the dimension 6 4-fermion operators that we are interested in. We will ignore these two terms in our analysis for $\mu - e$ conversion.

At $q^2 = 0$, we note that $f^Z_{L,R} \neq 0$. For practical purpose, following [30], we will evaluate the non-photonic form factors at $q^2 = -m^2_\mu$. The amplitude $\mathcal{M}_Z$ in (48) can be reproduced by the following Fermi interaction

$$\mathcal{L}_{Z,\text{eff}} = \frac{G_F}{\sqrt{2}}\Big[f^Z_L(-m^2_\mu)\overline{e_L}\gamma_\mu\mu_L + f^Z_R(-m^2_\mu)\overline{e_R}\gamma_\mu\mu_R\Big]\cdot\Big[\overline{q}\left(C^q_V\gamma^\mu + C^q_A\gamma^\mu\gamma_5\right)q\Big] + \cdots \tag{51}$$

where the $\cdots$ denotes non-local operators. Once again, matching (51) with the effective Lagrangian for $\mu - e$ conversion in Sec. 3, we obtain

$$\frac{C^{(q)Z}_{V(L,R)}(-m^2_\mu)}{\Lambda^2} = -\frac{G_F}{\sqrt{2}}\,C^q_V\,f^Z_{L,R}(-m^2_\mu)\,. \tag{52}$$

As a bonus, we also obtain the effective axial vector coupling

$$\frac{C^{(q)Z}_{A(L,R)}(-m^2_\mu)}{\Lambda^2} = -\frac{G_F}{\sqrt{2}}\,C^q_A\,f^Z_{L,R}(-m^2_\mu)\,, \tag{53}$$

which is nevertheless irrelevant for the coherent $\mu - e$ conversion processes in nuclei.

4.2.3. Scalar Higgs exchange

Now we consider the Feynman diagram in Fig. 2 for the CP-even scalar Higgs contributions to $\mu - e$ conversion. In the extended mirror fermion model [38], the physical neutral Higgses are mixtures of the neutral components from the two doublets Φ_2 and Φ_{2M} as well as the GM triplets ξ and $\tilde{\chi}$. They are denoted by $\tilde{H}_{1,2,3}$ with $\tilde{H}_1$ identified as the SM 125 GeV Higgs. In the limit of $|q^2| \ll m_{\tilde{H}_a}$, we obtain the following amplitude

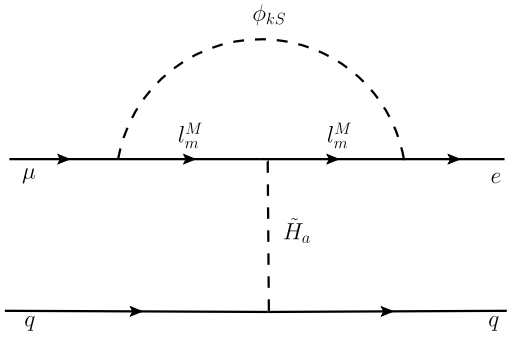

Fig. 2. One-loop induced Feynman diagram from CP-even scalar exchanges for $\mu - e$ conversion in the electroweak-scale ν_R model. Diagrams for external leg dressings are not shown.

$$\mathcal{M}_S \approx \frac{-m_q G_F}{\sqrt{2}\, s_2} \sum_{a=1}^{3} \frac{O_{a1}}{m^2_{\tilde{H}_a}} \Big[f_L^{Sa}(q^2) \overline{u_e}(p')\, P_L\, u_\mu(p) + f_R^{Sa}(q^2)\, \overline{u_e}(p') P_R\, u_\mu(p) \Big] \times \big[\overline{u_q}(k') u_q(k)\big], \tag{54}$$

where the $f_{L,R}^{Sa}(q^2)$ are the form factors given by

$$\begin{aligned} f_L^{Sa}(q^2) = {} & \frac{1}{8\pi^2} \frac{O_{a1}}{s_2(m_\mu^2 - m_e^2)} \sum_{k,m} \int_0^1 dx \\ & \Big\{ \Big[(1-x) m_\mu m_e \Big(m_e \mathcal{U}_{1m}^{R\,k} \Big(\mathcal{U}_{2m}^{R\,k}\Big)^* + m_\mu \mathcal{U}_{1m}^{L\,k} \Big(\mathcal{U}_{2m}^{L\,k}\Big)^* \Big) \\ & + M_m m_\mu m_e \mathcal{U}_{1m}^{L\,k} \Big(\mathcal{U}_{2m}^{R\,k}\Big)^* \Big] \log\left(\frac{\Delta_{km}^e(x)}{\Delta_{km}^\mu(x)} \right) \\ & + M_m \Big(m_\mu^2 \log(\Delta_{km}^e(x)) - m_e^2 \log(\Delta_{km}^\mu(x)) \Big) \mathcal{U}_{1m}^{R\,k} \Big(\mathcal{U}_{2m}^{L\,k}\Big)^* \Big\} \\ & + \frac{1}{8\pi^2} \frac{O_{a2}}{s_{2M}} \sum_{k,m} \int_0^1 \int_0^{1-x} dx dy\, M_m \Big\{ (-1 - 2\log(\Delta_{km}(q^2))) \mathcal{U}_{1m}^{R\,k} \Big(\mathcal{U}_{2m}^{L\,k}\Big)^* \\ & - \frac{1}{M_m \Delta_{km}(q^2)} \Big[m_\mu (1-2y) \mathcal{U}_{1m}^{R\,k} \Big(\mathcal{U}_{2m}^{R\,k}\Big)^* \\ & + m_e (1-2x) \mathcal{U}_{1m}^{L\,k} \Big(\mathcal{U}_{2m}^{L\,k}\Big)^* \Big] \\ & - \frac{1}{M_m^2 \Delta_{km}(q^2)} \Big[m_\mu m_e (1-x-y) \mathcal{U}_{1m}^{L\,k} \Big(\mathcal{U}_{2m}^{R\,k}\Big)^* \Big] \\ & + \frac{1}{M_m^2 \Delta_{km}(q^2)} \Big[(1-x-y) \Big(m_\mu^2 y + m_e^2 x \Big) + xyq^2 \\ & - M_m^2 \Big] \mathcal{U}_{1m}^{R\,k} \Big(\mathcal{U}_{2m}^{L\,k}\Big)^* \Big\}, \end{aligned} \tag{55}$$

and $f_R^{Sa}(q^2)$ can be obtained from $f_L^{Sa}(q^2)$ with $L \leftrightarrow R$ for all the quantities with L, R subscripts or superscripts. Here we have $s_2 = v_2/v$ and $s_{2M} = v_{2M}/v$ where v_2 and v_{2M} are the VEVs of two doublets Φ_2 and Φ_{2M} respectively, and together with the VEV v_M of the triplet scalar $\tilde{\chi}$, they satisfy the constraint $v_2^2 + v_{2M}^2 + 8v_M^2 = v^2$ where $v \approx 246$ GeV. O_{a1} and O_{a2} are the first and second columns of the Higgs mixing matrix defined in (42) of [38].

The amplitude $\mathcal{M}_S$ in (54) can be reproduced by the following interaction

$$\mathcal{L}_{S,\text{eff}} = \frac{-m_q G_F}{\sqrt{2}\, s_2} \sum_{a=1}^{3} \frac{O_{a1}}{m^2_{\tilde{H}_a}} \left[f_L^{Sa}(q^2) \overline{e}\, P_L\, \mu + f_R^{Sa}(q^2)\, \overline{e}\, P_R\, \mu \right] \cdot [\overline{q}\, q]\ . \tag{56}$$

Comparing this Lagrangian (56) with the effective Lagrangian for $\mu - e$ conversion in Sec. 3, we can obtain

$$\frac{C^{(q)H}_{S(L,R)}(-m_\mu^2)}{\Lambda^2} = \frac{1}{\sqrt{2}\, s_2\, m_\mu} \sum_{a=1}^{3} \frac{O_{a1}}{m^2_{\tilde{H}_a}}\, f^{Sa}_{L,R}(-m_\mu^2)\ . \tag{57}$$

Since we are concentrating on the coherent conversion processes in which the final state of the nucleus $|N'\rangle$ is the same as the initial one $|N\rangle$, we will ignore the contributions from the CP-odd Higgses which give rise to vanishing matrix element $\langle N'|\bar{q}\gamma_5 q|N\rangle$ if $|N'\rangle = |N\rangle$.

4.2.4. Box diagrams

First, in analogy with the lepton sector, we will write down the relevant A_4 invariant Yukawa interactions of quarks in the mirror fermion model,

$$\mathcal{L}_{Yq} \supset - \sum_{q=u,d} \sum_{k=0}^{3} \sum_{i,j=1}^{3} \overline{q}_i \left\{ \mathcal{V}_{ij}^{Lqk} P_R + \mathcal{V}_{ij}^{Rqk} P_L \right\} q_j^M\, \phi_{kS} + \text{H.c.}\,. \tag{58}$$

where

$$\begin{aligned} \mathcal{V}^{Lqk} &\equiv V_L^{q\,\dagger} M^{Q,k} V_R^{q^M}\ , \\ \mathcal{V}^{Rqk} &\equiv V_R^{q\,\dagger} M^{q,k} V_L^{q^M}\ . \end{aligned} \tag{59}$$

Here $V^u_{L,R}$, $V^d_{L,R}$, $V^{u^M}_{L,R}$, $V^{d^M}_{L,R}$, are the unitary matrix which transform the fields to the physical basis

$$u_{L,0} = V_L^u u_L,\ d_{L,0} = V_L^d d_L,\ u^M_{L,0} = V_L^{u^M} u^M_L,\ d^M_{L,0} = V_L^{d^M} d^M_L,$$

and

$$u_{R,0} = V_R^u u_R,\ d_{R,0} = V_R^d d_R,\ u^M_{R,0} = V_R^{u^M} u^M_R,\ d^M_{R,0} = V_R^{d^M} d^M_R.$$

The $M^{Q,k}$ in (59) are 3×3 matrices which are given by

$$\begin{aligned} M^{Q,0} &= \begin{pmatrix} g^Q_{0S} & 0 & 0 \\ 0 & g^Q_{0S} & 0 \\ 0 & 0 & g^Q_{0S} \end{pmatrix} \quad , \quad M^{Q,1} = \begin{pmatrix} 0 & 0 & 0 \\ 0 & 0 & g^Q_{1S} \\ 0 & g^Q_{2S} & 0 \end{pmatrix}, \\ M^{Q,2} &= \begin{pmatrix} 0 & 0 & g^Q_{2S} \\ 0 & 0 & 0 \\ g^Q_{1S} & 0 & 0 \end{pmatrix} \quad , \quad M^{Q,3} = \begin{pmatrix} 0 & g^Q_{1S} & 0 \\ g^Q_{2S} & 0 & 0 \\ 0 & 0 & 0 \end{pmatrix}, \end{aligned} \tag{60}$$

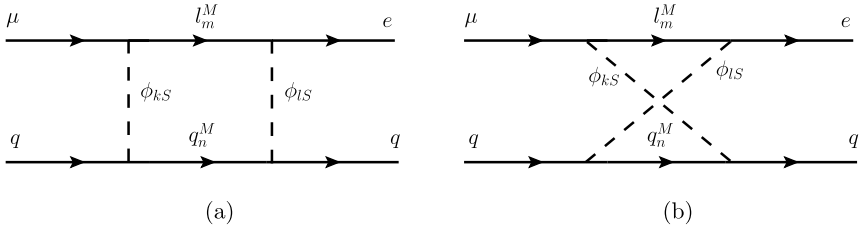

Fig. 3. Box diagrams.

and similar decompositions for $M^{u,k}$ and $M^{d,k}$ in (59) can be obtained by the substitutions of $g_{iS}^{Q} \to g_{iS}^{u}$ and g_{iS}^{d} respectively in (60).

The amplitude for box diagram contributions from Fig. 3 is given by

$$\begin{aligned}\mathcal{M}_B = &\Big(f_{VL}^{Bq}\,\overline{u}_{Le}(p_2)\gamma_\mu u_{L\mu}(p_1) + f_{VR}^{Bq}\,\overline{u}_{Re}(p_2)\gamma_\mu u_{R\mu}(p_1)\Big)\overline{u}_q(p_4)\gamma^\mu u_q(p_3)\\ &+\Big(f_{SL}^{Bq}\,\overline{u}_e(p_2)P_L u_\mu(p_1) + f_{SR}^{Bq}\,\overline{u}_e(p_2)P_R u_\mu(p_1)\Big)\overline{u}_q(p_4)u_q(p_3) + \cdots\,,\end{aligned} \tag{61}$$

where the $\cdots$ denotes non-local operators. In the limit of $m_e\,, m_\mu\,, m_q \ll M_m\,, M_n$, the $f_{VL,VR}^{Bq}$ are given by

$$\begin{aligned} f_{VL}^{Bq} &= \frac{1}{64\pi^2}\sum_{k,l}\sum_{i,n,m}\Big(\mathcal{V}_{in}^{Lq\,l}\Big(\mathcal{V}_{in}^{Lq\,k}\Big)^* - \mathcal{V}_{in}^{Lq\,k}\Big(\mathcal{V}_{in}^{Lq\,l}\Big)^* + \mathcal{V}_{in}^{Rq\,l}\Big(\mathcal{V}_{in}^{Rq\,k}\Big)^*\\ &\quad - \mathcal{V}_{in}^{Rq\,k}\Big(\mathcal{V}_{in}^{Rq\,l}\Big)^*\Big)\times\Big(\mathcal{U}_{1m}^{L\,l}\Big(\mathcal{U}_{2m}^{L\,k}\Big)^*\Big)\frac{1}{M_m^2}\mathcal{I}_{n,m}^{k,l}\\ &= 0\,,\\ f_{VR}^{Bq} &= \frac{1}{64\pi^2}\sum_{k,l}\sum_{i,n,m}\Big(\mathcal{V}_{in}^{Lq\,l}\Big(\mathcal{V}_{in}^{Lq\,k}\Big)^* - \mathcal{V}_{in}^{Lq\,k}\Big(\mathcal{V}_{in}^{Lq\,l}\Big)^* + \mathcal{V}_{in}^{Rq\,l}\Big(\mathcal{V}_{in}^{Rq\,k}\Big)^*\\ &\quad - \mathcal{V}_{in}^{Rq\,k}\Big(\mathcal{V}_{in}^{Rq\,l}\Big)^*\Big)\times\Big(\mathcal{U}_{1m}^{R\,l}\Big(\mathcal{U}_{2m}^{R\,k}\Big)^*\Big)\frac{1}{M_m^2}\mathcal{I}_{n,m}^{k,l}\,,\\ &= 0\,, \end{aligned} \tag{62}$$

and the $f_{SL,SR}^{Bq}$ are given by

$$\begin{aligned} f_{SL}^{Bq} &= \frac{1}{32\pi^2}\sum_{k,l}\sum_{i,n,m} M_m M_n\Big(\mathcal{V}_{in}^{Lq\,l}\Big(\mathcal{V}_{in}^{Rq\,k}\Big)^* + \mathcal{V}_{in}^{Lq\,k}\Big(\mathcal{V}_{in}^{Rq\,l}\Big)^* + \mathcal{V}_{in}^{Rq\,l}\Big(\mathcal{V}_{in}^{Lq\,k}\Big)^*\\ &\quad - \mathcal{V}_{in}^{Rq\,k}\Big(\mathcal{V}_{in}^{Lq\,l}\Big)^*\Big)\times\Big(\mathcal{U}_{1m}^{R\,l}\Big(\mathcal{U}_{2m}^{L\,k}\Big)^*\Big)\frac{1}{M_m^4}\mathcal{J}_{n,m}^{k,l}\,,\\ f_{SR}^{Bq} &= \frac{1}{32\pi^2}\sum_{k,l}\sum_{i,n,m} M_m M_n\Big(\mathcal{V}_{in}^{Lq\,l}\Big(\mathcal{V}_{in}^{Rq\,k}\Big)^* + \mathcal{V}_{in}^{Lq\,k}\Big(\mathcal{V}_{in}^{Rq\,l}\Big)^* + \mathcal{V}_{in}^{Rq\,l}\Big(\mathcal{V}_{in}^{Lq\,k}\Big)^*\\ &\quad - \mathcal{V}_{in}^{Rq\,k}\Big(\mathcal{V}_{in}^{Lq\,l}\Big)^*\Big)\times\Big(\mathcal{U}_{1m}^{L\,l}\Big(\mathcal{U}_{2m}^{R\,k}\Big)^*\Big)\frac{1}{M_m^4}\mathcal{J}_{n,m}^{k,l}\,. \end{aligned} \tag{63}$$

Here, the two functions $\mathcal{I}_{n,m}^{k,l}$ and $\mathcal{J}_{n,m}^{k,l}$ are defined as follows

$$\mathcal{I}^{k,l}_{n,m} = \int_0^1 \int_0^{1-x_1} \int_0^{1-x_1-x_2} dx_1 dx_2 dx_3 \times \left(\frac{1}{r_{nm} + x_1 (r_{km} - r_{nm}) + x_2 (1 - r_{nm}) + x_3 (r_{lm} - r_{nm})} \right) ,$$
$$\mathcal{J}^{k,l}_{n,m} = \int_0^1 \int_0^{1-x_1} \int_0^{1-x_1-x_2} dx_1 dx_2 dx_3 \times \left(\frac{1}{r_{nm} + x_1 (r_{km} - r_{nm}) + x_2 (1 - r_{nm}) + x_3 (r_{lm} - r_{nm})} \right)^2 , \quad (64)$$

with $r_{nm} = M_n^2/M_m^2$, $r_{km} = m_k^2/M_m^2$ and $r_{lm} = m_l^2/M_m^2$. If one ignores further the tiny masses of the Higgs singlets m_k and m_l as compared with the mirror lepton mass M_m and mirror quark mass M_n in the above integrals, we set $r_{km} = r_{lm} = 0$ and obtain

$$\mathcal{I}^{k,l}_{n,m} = -\frac{\log r_{nm}}{2(1 - r_{nm})} , \qquad \mathcal{J}^{k,l}_{n,m} = -\frac{1 - r_{nm} - \log r_{nm}}{r_{nm}(1 - r_{nm})} . \quad (65)$$

The amplitude in (61) can be reproduced by the following Lagrangian

$$\mathcal{L}_{\text{Box,eff}} = \left[f^{Bq}_{VL} \bar{e} \gamma_\mu P_L \mu + f^{Bq}_{VR} \bar{e} \gamma_\mu P_R \mu \right] \cdot \bar{q} \gamma^\mu q + \left[f^{Bq}_{SL} \bar{e} P_L \mu + f^{Bq}_{SR} \bar{e} P_R \mu \right] \cdot \bar{q} q . \quad (66)$$

Matching with the effective Lagrangian in Sec. 3, we get the following box contributions,

$$\frac{C^{(q)Box}_{V(L,R)}(0)}{\Lambda^2} = -f^{Bq}_{VL,VR} = 0 , \qquad \frac{C^{(q)Box}_{S(L,R)}(0)}{\Lambda^2} = -\frac{1}{m_\mu m_q} f^{Bq}_{SL,SR} . \quad (67)$$

We can summarize the four fermion coupling coefficients we have computed for the extended mirror fermion model from the photon, Z-boson, Higgses and box diagrams. The total contributions to $C^{(q)}_{V(L,R)}$ and $C^{(q)}_{S(L,R)}$ are given by

$$C^{(q)}_{V(L,R)} \approx C^{(q)\gamma}_{V(L,R)}(0) + C^{(q)Z}_{V(L,R)}(-m_\mu^2) + C^{(q)Box}_{V(L,R)}(0) , \qquad C^{(q)}_{S(L,R)} \approx C^{(q)H}_{S(L,R)}(-m_\mu^2) + C^{(q)Box}_{S(L,R)}(0) . \quad (68)$$

We note that the box diagrams have vanishing contributions to the vector coupling coefficients.

4.3. Two loop gluonic diagram

We also calculate the two loop gluonic contributions from Fig. 4. Once again, in the limit of $|q^2| \ll m_{\tilde{H}_a}$, we obtain the following amplitude

$$\mathcal{M}_G = \frac{G_F \alpha_s}{2\sqrt{2}\pi} \sum_{a=1}^{3} \frac{1}{m^2_{\tilde{H}_a}} \left[f^{Ga}_L(q^2) \overline{u_e}(p') P_L u_\mu(p) + f^{Ga}_R(q^2) \overline{u_e}(p') P_R u_\mu(p) \right] \times \left(k^\mu k'^\nu - g^{\mu\nu} k k' \right) \delta^{\alpha\beta} \epsilon^{\alpha *}_\mu(k') \epsilon^{\beta *}_\nu(k) , \quad (69)$$

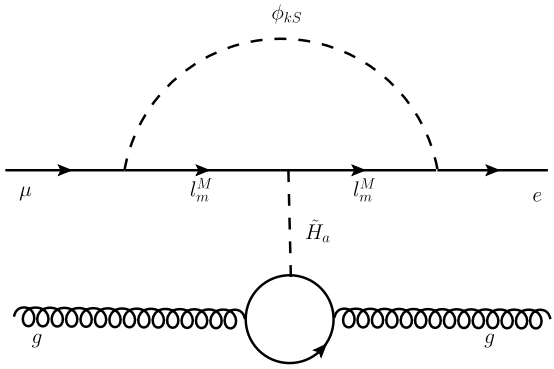

Fig. 4. A two-loop induced Feynman diagram from scalar and gluonic exchanges for $\mu - e$ conversion in the electroweak-scale ν_R model. Diagrams for external leg dressings are not shown.

where $\alpha_s = g_s^2/4\pi$ with g_s being the strong coupling constant and $f_{L,R}^{Ga}(q^2)$ are the form factors given by

$$f_{L,R}^{Ga}(q^2) = \left(\frac{O_{a1}}{s_2}\, \mathcal{G}(\tau_t) + \sum_n \left(\frac{O_{a2}}{s_{2M}} \mathcal{G}(\tau_n) \right) \right) \times f_{L,R}^{Sa}(q^2)\,. \tag{70}$$

Here $\tau_t = \frac{q^2}{m_t^2}$, $\tau_n = \frac{q^2}{M_n^2}$ and m_t, M_n are the masses of top quark and mirror quarks respectively. The integral function $\mathcal{G}(\tau)$ is defined as

$$\begin{aligned} \mathcal{G}(\tau) &= \int_0^1 dx \int_0^{1-x} dy\, \frac{1-4xy}{1-xy\tau}\,, \\ &= \frac{1}{\tau^2} \left\{ 2\tau + (\tau-4) \left[\mathrm{Li}_2 \left(\frac{1}{2} \left(\tau + \sqrt{\tau\,(\tau-4)} \right) \right) + \mathrm{Li}_2 \left(\frac{1}{2} \left(\tau - \sqrt{\tau\,(\tau-4)} \right) \right) \right] \right\}, \end{aligned} \tag{71}$$

where $\mathrm{Li}_2(z)$ is the dilogarithm function.

The amplitude $\mathcal{M}_G$ in (69) can be reproduced by the following interaction

$$\mathcal{L}_{G,\mathrm{eff}} = \frac{G_F \alpha_s}{2\sqrt{2}\,\pi} \sum_{a=1}^{3} \frac{1}{m_{\tilde{H}_a}^2} \left[f_L^{Ga}(q^2)\, \overline{e}\, P_L\, \mu + f_R^{Ga}(q^2)\, \overline{e} P_R\, \mu \right] G^{\alpha}_{\mu\nu}\, G^{\alpha\mu\nu}. \tag{72}$$

Once again, we compare this Lagrangian (72) with the effective Lagrangian for $\mu - e$ conversion in Sec. 3, we can read off

$$\frac{C_{GQ(L,R)}}{\Lambda^2} = \frac{-g_s^3 \alpha_s}{\sqrt{2}\,\pi\, m_\mu \beta_L} \sum_{a=1}^{3} \frac{1}{m_{\tilde{H}_a}^2} \left(f_{R,L}^{Ga}(-m_\mu^2) \right), \tag{73}$$

where β_L is the QCD beta-function of 3 light flavors.

4.4. Other two loop diagrams

Replacing the two gluons in Fig. 4, one can obtain another two loop photonic diagram. However, the contribution from this photonic two loop diagram is smaller than that coming from the

gluonic two loop diagram by a factor of $\alpha_{\rm em}/\alpha_s$. One can also consider replacing the scalar Higgs exchange in Fig. 4 by a neutral vector gauge boson exchange like the photon or the Z boson. For the resulting two loop diagrams, one needs to consider the effective γgg and Zgg vertices. For on-shell particles these vertices are vanishing due to the Landau–Yang theorem. Nevertheless there can be anomalous $\gamma^* g^* g^*$ and $Z^* g^* g^*$ couplings when at least one of the external gauge particles is off-shell. Anomalous $\gamma^*\gamma^*\gamma^*$ and $Z^*\gamma^*\gamma^*$ couplings had been studied before in [54]. One anticipates that similar analysis can be done for the anomalous $\gamma^* g^* g^*$ and $Z^* g^* g^*$ couplings as well. We will not perform such analysis here but just mention that the resulting two loop diagrams are necessarily smaller than the one loop diagram we are considering in Fig. 1. We will only consider the two loop Higgs exchange diagram in Fig. 4 since the one loop Higgs exchange diagram in Fig. 2 is suppressed by light quark masses.

We will also neglect the two loop gluonic diagrams from CP-odd Higgses since they would lead to effective operator $\tilde{G}^a_{\mu\nu} G^{a\mu\nu}$ whose matrix element $\langle N'|\tilde{G}^a_{\mu\nu} G^{a\mu\nu}|N\rangle$ is vanishing for coherent $\mu - e$ conversion with $|N'\rangle = |N\rangle$.

Finally, we note that dressing the quark line or connecting the lepton and quark lines in Fig. 1 by the SM neutral gauge bosons or Higgs will promote it into two loop diagrams. This class of two loop diagrams are not finite and renormalization is needed to carry out to achieve meaningful results. Such calculation is beyond the scope of this work.

5. The relationship between $\mu - e$ conversion and $\mu \to e\gamma$

We will show in the next section that the contributions to the four-fermion coupling coefficients from the photon, Z-boson, Higgses, gluonic and box diagrams are negligible compared with the photon contributions to the two dipole moment form factors. Here we will establish an useful relation between the $\mu - e$ conversion rate and the radiative decay rate of $\mu \to e\gamma$.

Since the momentum transfer q^2 in the $\mu - e$ conversion processes in nuclei is expected to be quite small, of order of m_μ^2, we can make a Taylor expansion for the form factors $f_{E0,M0}(q^2)$ and $f_{E1,M1}(q^2)$ of the photon contributions deduced in the previous Sec. 4 around $q^2 = 0$. For the contributions from the other form factors of the Z-boson and scalar Higgs exchanges, we will show that they are numerically small compared with the photon contributions in the next section. Thus for small q^2, we have

$$\begin{aligned} f_{E0,M0}(q^2) \approx \frac{q^2}{32\pi^2}\frac{1}{M_m^4}\sum_{k,m}\Big\{ & \left(\mathcal{U}^{Lk}_{1m}\left(\mathcal{U}^{Lk}_{2m}\right)^* \pm \mathcal{U}^{Rk}_{1m}\left(\mathcal{U}^{Rk}_{2m}\right)^*\right) \\ & \times\left[M_m^2\left(\mathcal{I}(r_{km}) + 2\mathcal{I}_{30}(r_{km})\right) \pm m_\mu m_e \mathcal{I}_{10}(r_{km})\right] \\ & + \left(\mathcal{U}^{Lk}_{1m}\left(\mathcal{U}^{Rk}_{2m}\right)^* \pm \mathcal{U}^{Rk}_{1m}\left(\mathcal{U}^{Lk}_{2m}\right)^*\right) M_m\left(m_\mu \pm m_e\right)\mathcal{I}_{20}(r_{km})\Big\}, \end{aligned} \tag{74}$$

and

$$\begin{aligned} f_{M1,E1}(q^2) \approx & -\frac{m_\mu}{32\pi^2}\sum_{k,m}\Big\{\frac{1}{M_m^2}\left(m_\mu \pm m_e\right)\left(\mathcal{U}^{Lk}_{1m}\left(\mathcal{U}^{Lk}_{2m}\right)^* \pm \mathcal{U}^{Rk}_{1m}\left(\mathcal{U}^{Rk}_{2m}\right)^*\right)\mathcal{I}(r_{km}) \\ & + \frac{1}{M_m}\left(\mathcal{U}^{Lk}_{1m}\left(\mathcal{U}^{Rk}_{2m}\right)^* \pm \mathcal{U}^{Rk}_{1m}\left(\mathcal{U}^{Lk}_{2m}\right)^*\right)\mathcal{J}(r_{km})\Big\} \\ & - \frac{m_\mu q^2}{32\pi^2}\Big\{\frac{1}{M_m^4}\left(m_\mu \pm m_e\right)\left(\mathcal{U}^{Lk}_{1m}\left(\mathcal{U}^{Lk}_{2m}\right)^* \pm \mathcal{U}^{Rk}_{1m}\left(\mathcal{U}^{Rk}_{2m}\right)^*\right)\mathcal{I}_{40}(r_{km}) \end{aligned}$$

$$+\frac{1}{M_m^3}\left(\mathcal{U}_{1m}^{L\,k}\left(\mathcal{U}_{2m}^{R\,k}\right)^* \pm \mathcal{U}_{1m}^{R\,k}\left(\mathcal{U}_{2m}^{L\,k}\right)^*\right)\mathcal{I}_{50}(r_{km})\Bigg\}\,. \tag{75}$$

Here $r_{km} = m_k^2/M_m^2$ and the expressions for the Feynman parameterization integrals $\mathcal{I}$, $\mathcal{J}$ and $\mathcal{I}_{i0}$ $(i = 1, 2, \cdots, 5)$ can be found in Appendix A.

From (26) in Sec. 3, the conversion rate (ignoring the scalar Higgs contributions which we will show they are negligible in the next section) is given by

$$\Gamma_{\rm conv} = \frac{m_\mu^5}{4\Lambda^4}\left(\left|C_{DR}D + 4\tilde{C}_{VR}^{(p)}V^{(p)}\right|^2 + \left|C_{DL}D + 4\tilde{C}_{VL}^{(p)}V^{(p)}\right|^2\right), \tag{76}$$

where $C_{DR,DL}$ are given by (43), $\tilde{C}_{VR,VL}^{(p)}$ are given by (27) in Sec. 3, and lastly, D and $V^{(p)}$ are the dimensionless overlap integrals of the relativistic wave functions of muon and electron. For convenience, in Table 3 of Sec. 3, we list the numerical values of D and $V^{(p)}$ for various nuclei given in [31]. To obtain (76), we have used the following result valid for the neutron,

$$\tilde{C}_{V(L,R)}^{(n)} = \sum_{u,d,s} C_{V(L,R)}^{(q)} f_{Vn}^{(q)} = 0\,. \tag{77}$$

Using the above approximate form factors (74) and (75) for small q^2, we can derive

$$\begin{aligned} C_{DR,DL}(q^2) \approx \frac{e\Lambda^2}{32\pi^2 m_\mu}\sum_{k,m}\Bigg\{ & \frac{\mathcal{I}(r_{km})}{M_m^2}\left(m_\mu \mathcal{U}_{1m}^{R,L\,k}\left(\mathcal{U}_{2m}^{R,L\,k}\right)^* + m_e \mathcal{U}_{1m}^{L,R\,k}\left(\mathcal{U}_{2m}^{L,R\,k}\right)^*\right) \\ & + \frac{\mathcal{J}(r_{km})}{M_m}\mathcal{U}_{1m}^{R,L\,k}\left(\mathcal{U}_{2m}^{L,R\,k}\right)^* \\ & + \frac{q^2}{M_m^2}\Bigg[\frac{\mathcal{I}_{40}(r_{km})}{M_m^2}\left(m_\mu \mathcal{U}_{1m}^{R,L\,k}\left(\mathcal{U}_{2m}^{R,L\,k}\right)^* \right. \\ & \qquad \left. + m_e \mathcal{U}_{1m}^{L,R\,k}\left(\mathcal{U}_{2m}^{L,R\,k}\right)^*\right) \\ & \qquad + \frac{\mathcal{I}_{50}(r_{km})}{M_m}\mathcal{U}_{1m}^{R,L\,k}\left(\mathcal{U}_{2m}^{L,R\,k}\right)^*\Bigg]\Bigg\}, \end{aligned} \tag{78}$$

and summing over the contributions from light quarks, we have (keeping only the contributions from the photon, since the Z contributions will be shown to be numerically insignificance in the next section)

$$\begin{aligned} \tilde{C}_{VL,VR}^{(p)} \approx \frac{e^2\Lambda^2}{16\pi^2 M_m^4}\sum_{k,m}\Bigg\{ & M_m^2\left(\mathcal{I}(r_{km}) + 2\,\mathcal{I}_{30}(r_{km})\right)\mathcal{U}_{1m}^{R,L\,k}\left(\mathcal{U}_{2m}^{R,L\,k}\right)^* \\ & + m_\mu m_e \mathcal{I}_{10}(r_{km})\,\mathcal{U}_{1m}^{L,R\,k}\left(\mathcal{U}_{2m}^{L,R\,k}\right)^* \\ & + M_m \mathcal{I}_{20}(r_{km})\left(m_\mu \mathcal{U}_{1m}^{R,L\,k}\left(\mathcal{U}_{2m}^{L,R\,k}\right)^* + m_e \mathcal{U}_{1m}^{L,R\,k}\left(\mathcal{U}_{2m}^{R,L\,k}\right)^*\right)\Bigg\}. \end{aligned} \tag{79}$$

Dropping the q^2 terms in $C_{DR,DL}$ and keeping only those terms up to $\mathcal{O}(1/M_m^2)$ in $\tilde{C}_{VL,VR}^{(p)}$, we obtain the conversion rate from the photon contribution

$$\Gamma_{\rm conv}(q^2 \to 0) \approx \frac{m_\mu^5}{4}\frac{1}{(32\pi^2)^2}$$

$$\times \sum_{k,m}\left\{\left|\frac{16\pi^2 D}{m_\mu}C_L^{km}+8V^{(p)}e^2\frac{\mathcal{I}(r_{km})+2\,\mathcal{I}_{30}(r_{km})}{M_m^2}\mathcal{U}_{1m}^{L\,k}\left(\mathcal{U}_{2m}^{L\,k}\right)^*\right|^2\right. \quad (80)$$
$$\left.+\left|\frac{16\pi^2 D}{m_\mu}C_R^{km}+8V^{(p)}e^2\frac{\mathcal{I}(r_{km})+2\,\mathcal{I}_{30}(r_{km})}{M_m^2}\mathcal{U}_{1m}^{R\,k}\left(\mathcal{U}_{2m}^{R\,k}\right)^*\right|^2\right\},$$

where

$$C_{L,R}^{km}=\frac{e}{16\pi^2}\left\{\frac{\mathcal{I}(r_{km})}{M_m^2}\left(m_\mu\mathcal{U}_{1m}^{R,L\,k}\left(\mathcal{U}_{2m}^{R,L\,k}\right)^*+m_e\mathcal{U}_{1m}^{L,R\,k}\left(\mathcal{U}_{2m}^{L,R\,k}\right)^*\right)\right.$$
$$\left.+\frac{\mathcal{J}(r_{km})}{M_m}\mathcal{U}_{1m}^{R,L\,k}\left(\mathcal{U}_{2m}^{L,R\,k}\right)^*\right\}. \quad (81)$$

Recall that for the on-shell process $\mu\to e\gamma$, we have [18]

$$\Gamma_{\mu\to e\gamma}=\frac{1}{16\pi}m_\mu^3\sum_{k,m}\left(|C_L^{km}|^2+|C_R^{km}|^2\right). \quad (82)$$

Thus, one obtains

$$\Gamma_{\rm conv}(q^2\to 0)\approx\pi D^2\Gamma_{\mu\to e\gamma}+\frac{m_\mu^5}{(64\pi^2)^2}\sum_{k,m}\left\{2DV^{(p)}\,(8\pi e)^2\,\frac{\mathcal{I}(r_{km})+2\mathcal{I}_{30}(r_{km})}{m_\mu M_m^2}\right.$$
$$\times\left(C_L^{km}\mathcal{U}_{1m}^{L\,k}\left(\mathcal{U}_{2m}^{L\,k}\right)^*+\left(C_L^{km}\right)^*\left(\mathcal{U}_{1m}^{L\,k}\right)^*\mathcal{U}_{2m}^{L\,k}\right.$$
$$\left.+C_R^{km}\mathcal{U}_{1m}^{R\,k}\left(\mathcal{U}_{2m}^{R\,k}\right)^*+\left(C_R^{km}\right)^*\left(\mathcal{U}_{1m}^{R\,k}\right)^*\mathcal{U}_{2m}^{R\,k}\right) \quad (83)$$
$$\left.+\left(8V^{(p)}e^2\frac{\mathcal{I}(r_{km})+2\mathcal{I}_{30}(r_{km})}{M_m^2}\right)^2\left(|\mathcal{U}_{1m}^{L\,k}\left(\mathcal{U}_{2m}^{L\,k}\right)^*|^2+|\mathcal{U}_{1m}^{R\,k}\left(\mathcal{U}_{2m}^{R\,k}\right)^*|^2\right)\right\}.$$

Note that since $C_{L,R}^{km}$ is scaled by $1/M_m$, the first, second and the third terms in (83) are scaled by m_μ^3/M_m^2, m_μ^4/M_m^3 and m_μ^5/M_m^4 respectively. Typically the first term in (83) is about 10^3 and 10^6 times larger than the second and the third terms respectively. If one drops the last two suppressed terms compared with the first one in (83), one obtains a simple relation

$$\Gamma_{\rm conv}(q^2\to 0)\approx\pi D^2\Gamma_{\mu\to e\gamma}. \quad (84)$$

Thus,

$$B_{\mu N\to eN}=\frac{\Gamma_{\rm conv}}{\Gamma_{\rm capt}}\approx\pi D^2\frac{\Gamma_\mu}{\Gamma_{\rm capt}}B_{\mu\to e\gamma}, \quad (85)$$

where Γ_μ is the total decay width of the muon.

6. Numerical analysis

In our analysis, we adopt the same assumptions for the parameter space as was done in [18]. We summarize them as follows.

- For the mass parameters, we take the masses of the singlet scalars ϕ_{kS} to be

$$m_0:m_1:m_2:m_3=M_S:2M_S:3M_S:4M_S, \quad (86)$$

where the common mass M_S is set to be 10 MeV; and for the mirror lepton masses, we set

$$M_m = M_{\text{mirror}} + \delta_m \tag{87}$$

where $\delta_1 = 0$, $\delta_2 = 10$ GeV, $\delta_3 = 20$ GeV and the common mass M_{mirror} is varied in the range of $100 - 800$ GeV. Our results are insensitive to these choices as long as $m_k/M_m \ll 1$.

- Note that the relations $g_{2S} = (g_{1S})^*$ and $g'_{2S} = (g'_{1S})^*$ hold due to the reality of the eigenvalues of the neutrino Dirac mass matrix. However, all the Yukawa couplings g_{0S}, g_{1S}, g_{2S}, g'_{0S}, g'_{1S}, and g'_{2S} are assumed to be real in our analysis. In general these Yukawa couplings for the lepton sector as well as the corresponding ones in the quark sector can be complex. They will then lead to non-vanishing electric dipole moments for the electron [55] and the neutron [56].
- Out of the four mixing matrices, only the one U_{PMNS} associated with the left-handed SM fermions are known. Following [18], we will consider two scenarios below:
  - Scenario 1: $U^M_{\text{PMNS}} = U'_{\text{PMNS}} = U'^M_{\text{PMNS}} = U^\dagger_{\text{CW}}$
  - Scenario 2: $U^M_{\text{PMNS}} = U'_{\text{PMNS}} = U'^M_{\text{PMNS}} = U_{\text{PMNS}}$

  where U_{CW} is given by (12). For the PMNS mixing matrix, we will use the best fit result in (3). In the two scenarios that we are studying, our results do not depend sensitively on the mass hierarchies.
- We will study the following two cases for the Yukawa couplings.
  1. $g_{0S} = g'_{0S}$ and $g_{1S} = g'_{1S} = 10^{-2} g_{0S}$. Hence the contributions from the A_4 triplet is small.
  2. $g_{0S} = g'_{0S} = g_{1S} = g'_{1S}$. Both A_4 singlet and triplet terms carry the same weight.
- For the parameters in the Higgs sector, we consider two cases studied in [38]:
  1. SM-like case (Eq. (50) of [38]) with the following mixing matrix of the three CP-even Higgses

$$O = \begin{pmatrix} 0.998 & -0.0518 & -0.0329 \\ 0.0514 & 0.999 & -0.0140 \\ 0.0336 & 0.0123 & 0.999 \end{pmatrix}, \tag{88}$$

     $s_2 = 0.92$, $s_{2M} = 0.16$ and the masses of the three CP-even Higgses are $m_{\tilde{H}_1} = 125.7$ GeV, $m_{\tilde{H}_2} = 420$ GeV and $m_{\tilde{H}_3} = 601$ GeV. Note that $\tilde{H}_1$ is basically SM-like in this case.
  2. SM-unlike case (row 13, Table 4 of [38]) with the following mixing matrix of the three CP-even Higgses

$$O = \begin{pmatrix} 0.131 & 0.075 & 0.985 \\ 0.979 & 0.146 & -0.141 \\ 0.155 & -0.986 & 0.054 \end{pmatrix}, \tag{89}$$

     $s_2 = 0.3$, $s_{2M} = 0.93$ and the masses of the three CP-even Higgses are $m_{\tilde{H}_1} = 125.1$ GeV, $m_{\tilde{H}_2} = 415$ GeV and $m_{\tilde{H}_3} = 906$ GeV. In this case, $\tilde{H}_1$ is a mixture of three CP-even Higgses in the model, with the SM Higgs is only a subdominant component [38].

From (26) in Sec. 3, we see that the $\mu - e$ conversion rate is determined by the following dimensionless coupling coefficients $C_{DL,DR}$, $\tilde{C}^{(p,n)}_{VL,VR}$ and $\tilde{C}^{(p,n)}_{SL,SR}$ with $C_{DL,DR}$ given by (43), and the latter two quantities defined in (27) and (29) respectively in Sec. 3 as well.

In Fig. 5, we plot the dipole coupling coefficients of the photon $|C_{DL}|/\Lambda^2$, $|C_{DR}|/\Lambda^2$ versus the common mirror lepton mass M_{mirror} varied from 100 to 800 GeV, while all the Yukawa couplings are simply set to be the same as 10^{-3}.

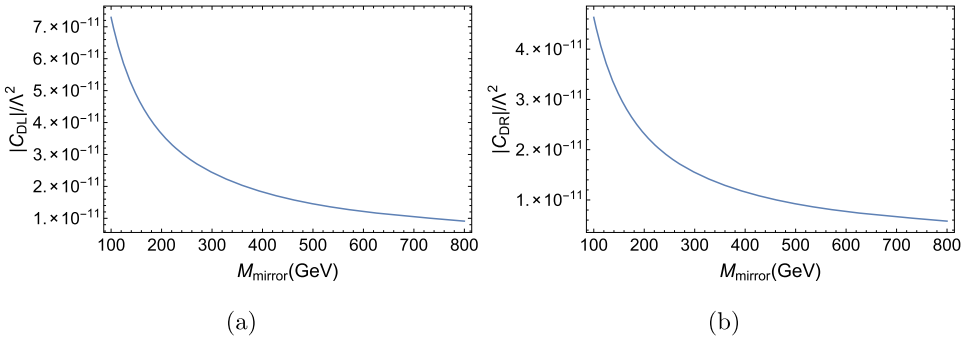

Fig. 5. The dipole coupling coefficients of the photon versus the common mirror lepton mass. All the Yukawa couplings are set to be the same as 10^{-3}.

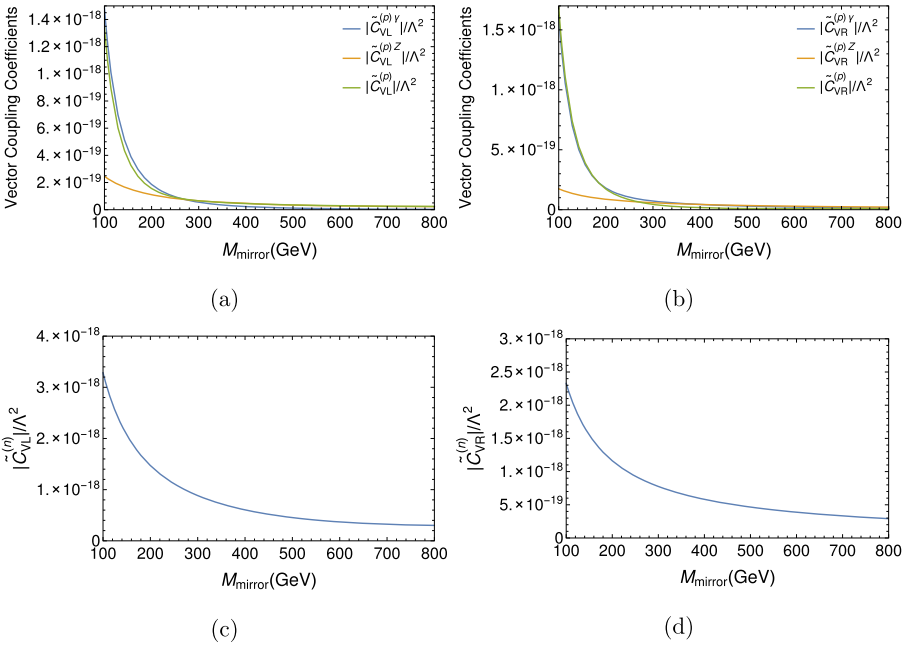

Fig. 6. The vector coupling coefficients for the proton and neutron versus the common mirror lepton mass. All the Yukawa couplings are set to be the same as 10^{-3}. Note that, the vector couplings coefficients for the neutron arise only from Z diagrams. (For interpretation of the colours in the figure(s), the reader is referred to the web version of this article.)

In Fig. 6, we plot the vector coupling coefficients $|\tilde{C}^{(p)}_{VL,VR}|/\Lambda^2$ for the proton (upper panel) and $|\tilde{C}^{(n)}_{VL,VR}|/\Lambda^2$ for the neutron (lower panel) versus M_{mirror} with all the Yukawa couplings set to be 10^{-3}. For the proton case, the individual contributions from the photon (blue) and Z (orange) contributions as well as their sums $|\tilde{C}^{(p)}_{VL,VR}|/\Lambda^2 = |\tilde{C}^{(p),\gamma}_{VL,VR} + \tilde{C}^{(p),Z}_{VL,VR}|/\Lambda^2$ are shown. For $\tilde{C}^{(p)}_{VL}$ in Fig. 6a, it is clear that as $M_{\text{mirror}} \leq 270$ GeV, there are destructive interferences between the photon and Z contributions. Photon contributions dominate for $M_{\text{mirror}} \leq 270$ GeV, while Z contributions dominate for $M_{\text{mirror}} \geq 270$ GeV. For $\tilde{C}^{(p)}_{VR}$ in Fig. 6b, Z contributions

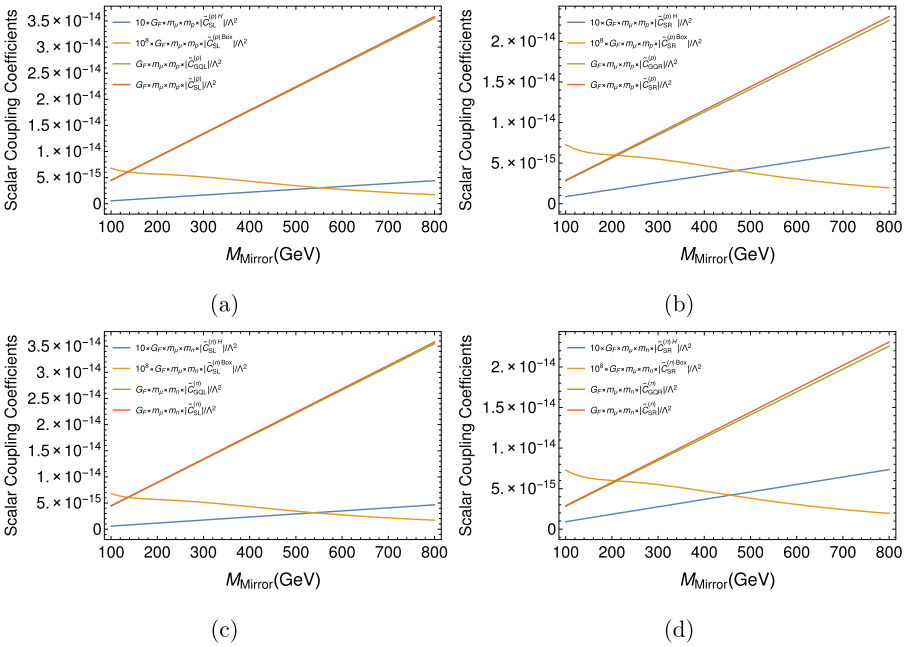

Fig. 7. The scalar coupling coefficients and gluonic coefficients for the proton and neutron versus the common mirror lepton mass for the SM-like case. All the Yukawa couplings are set to be the same as 10^{-3} and all mirror quark masses are set to be 500 GeV.

dominate only when $M_{\text{mirror}} \geq 400$ GeV, and the interferences are always destructive. For the neutron case in Figs. 6c and 6d, only the Z exchange diagrams contribute. Photon's contributions vanish for the neutron here due to (47) and (77).

In Figs. 7 and 8, we plot the scalar coupling coefficients $G_F m_\mu m_{p,n} |\tilde{C}^{(p,n)}_{SL,SR}|/\Lambda^2$ and their individual contributions from the Higgses, box and gluonic diagrams for the proton (upper panel) and neutron (lower panel) versus M_{mirror} for the SM-like and SM-unlike cases respectively. All the new Yukawa couplings including both lepton and quark sectors are again set to be the same as 10^{-3} and all mirror quark masses are set to be 500 GeV. Note that in order to show the Higgses and box contributions in the plots we have multiplied them by a factor of 10 and 10^8 respectively and hence they are really minuscule, compared with the gluonic two-loop diagram. The box contributions are particularly small since their amplitudes are proportional to the quartic power of the small Yukawa couplings, two from the lepton line and two from the quark line. Comparing Figs. 7 and 8 with Fig. 6, we see the vector couplings coefficients are about 4 to 5 order of magnitudes smaller than the gluonic contributions.

As mentioned above, the couplings coefficients plotted in Figs. 5, 6, 7 and 8 entered in the conversion rate formula (26). They are multiplied by appropriate dimensionless overlap integrals for various nuclei, which have more or less the same magnitude as listed in Table 3 in Sec. 3. Thus by comparison of these three plots it is clear that the dipole coupling coefficients $C_{DL,DR}$ in Figs. 5 from the photon diagrams are dominant over the other vector and scalar coupling coefficients $C_{VL,VR}$ and $C_{SL,SR}$ as well as the gluonic coefficient $C_{GQL,GQR}$ given in Figs. 6, 7 and 8. It is then justified to use our simple relation (85) in the subsequent numerical analysis for the conversion rate.

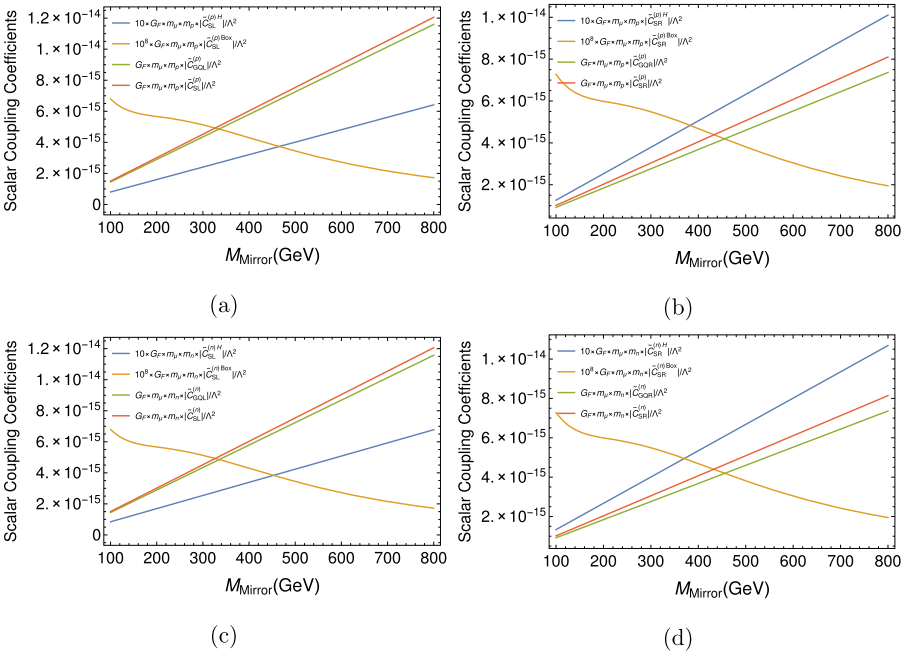

Fig. 8. Same as Fig. (7) for the SM-unlike case.

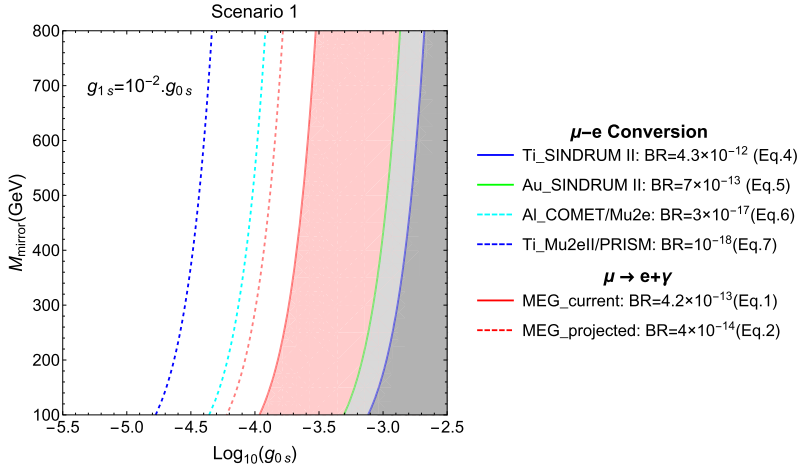

Fig. 9. Contour plots of $B(\mu - e$ conversion) and $B(\mu \to e\gamma)$ on the $(\log_{10}(g_{0S}), M_{\text{mirror}})$ plane for normal mass hierarchy in Scenario 1 with $g_{0S} = g'_{0S}$ and $g_{1S} = g'_{1S} = 10^{-2} g_{0S}$. The legend shows current experimental limits and projected sensitivities from COMET, Mu2e, SINDRUM II, PRISM and MEG. For details of other input parameters, one can refer to the text in Sec. 6.

In Figs. 9, 10, 11 and 12, we plot the contours of $B(\mu - e$ conversion) and $B(\mu \to e\gamma)$ with γ dominance in the $(\log_{10}(g_{0S}), M_{\text{mirror}})$ plane for Scenarios 1 and 2 with the normal neutrino mass hierarchy for the 2 cases of couplings aforementioned respectively. The blue and green solid lines correspond to the current limits from SINDRUM II experiments for $\mu - e$ conversion

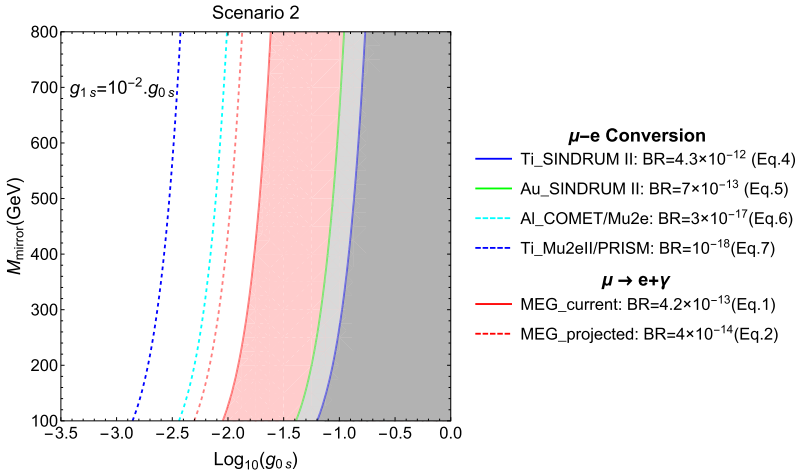

Fig. 10. Contour plots of $B(\mu - e$ conversion) and $B(\mu \to e\gamma)$ on the $(\log_{10}(g_{0S}), M_{\text{mirror}})$ plane for normal mass hierarchy in Scenario 2 with $g_{0S} = g'_{0S}$ and $g_{1S} = g'_{1S} = 10^{-2} g_{0S}$.

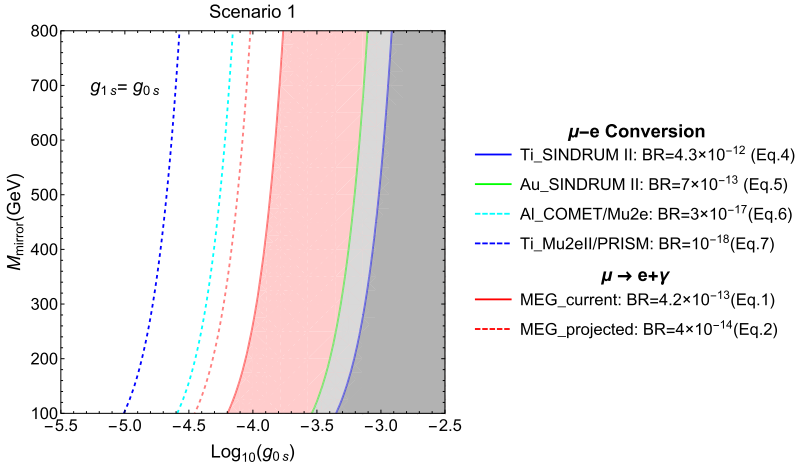

Fig. 11. Contour plots of $B(\mu - e$ conversion) and $B(\mu \to e\gamma)$ on the $(\log_{10}(g_{0S}), M_{\text{mirror}})$ plane for normal mass hierarchy in Scenario 1 with $g_{0S} = g'_{0S} = g_{1S} = g'_{1S}$.

to titanium (4) and gold (5) respectively. The red solid and dashed lines correspond to the current limit (1) and projected sensitivity (2) for $\mu \to e\gamma$ from MEG experiment. The cyan and blue dashed lines correspond to the projected sensitivities for $\mu - e$ conversion to aluminum and titanium from COMET, Mu2e (6) and Mu2e II, PRISM (7) experiments respectively.

Several comments are in order here regarding Figs. 9, 10, 11 and 12.

- We have studied in some details the effects of different settings of couplings on our results. Generally, we observe that as one varies the A_4 triplet coupling g_{1S} from $10^{-2} g_{0S}$ to g_{0S} (from Figs. 9 to 12) the contour plots for $B(\mu - e$ conversion) are shifted to the left. The

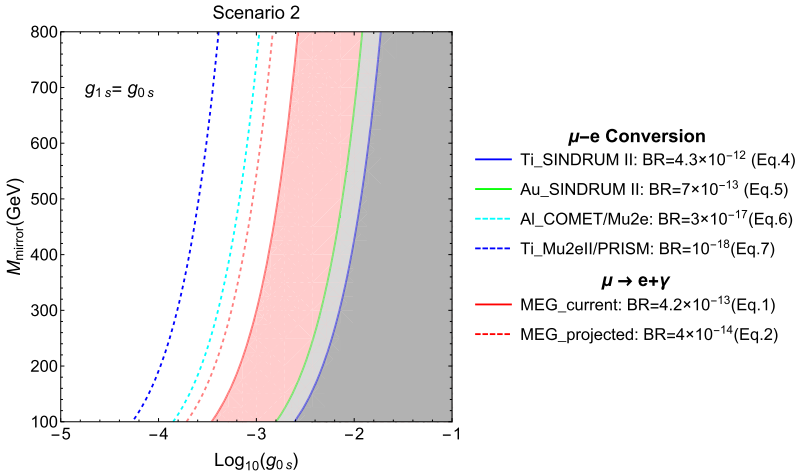

Fig. 12. Contour plots of $B(\mu - e$ conversion) and $B(\mu \to e\gamma)$ on the $(\log_{10}(g_{0S}), M_{\text{mirror}})$ plane for normal mass hierarchy in Scenario 2 with $g_{0S} = g'_{0S} = g_{1S} = g'_{1S}$.

A_4 triplet is playing a significant role in putting constraints on the parameter space for the CLFV processes, such as $\mu \to e\gamma$ and $\mu - e$ conversion in the model.

- For the sensitivity of the two scenarios, we find that
  - Generally, Scenario 2 is less constraining than Scenario 1.
  - In particular, when the A_4 singlet couplings are dominating (Figs. 9 and 10), Scenario 2 is less stringent than Scenario 1 by at least two order of magnitude. For instance, at $M_{\text{mirror}} = 200$ GeV, current limit from SINDRUM II for titanium (blue contours) implies the coupling $g_{0S} \leq 10^{-3}$ for Scenario 1 (Fig. 9), whereas for Scenario 2 (Fig. 10) we have $g_{0S} \leq 10^{-1}$. This is due to the fact that in Scenario 2, the three unknown unitary mixing matrices are now departure from U_{PMNS} which allows for larger effects since the amplitudes involve products of both the couplings and the elements of mixing matrices.
  - However, as one turns on the contribution from the A_4 triplet in Fig. 11 and Fig. 12, the discrepancy between two scenarios 1 and 2 shrink. Again, take $M_{\text{mirror}} = 200$ GeV, current limit from SINDRUM II for titanium (blue contours) implies the coupling $g_{0S,1S} \leq 10^{-3.2}$ for Scenario 1 (Fig. 11), whereas for Scenario 2 (Fig. 12) we have $g_{0S,1S} \leq 10^{-2.2}$. Comparing the four Figs. 9, 10, 11 and 12, we can see that Scenario 2 is more sensitive to the changes in the structure of A_4 couplings.
- From the four Figs. 9–12, we also see that the results show only weakly dependence on the mirror fermion masses. In Figs. 13 and 14, we pick the mirror fermion mass $M_{\text{mirror}} = 500$ GeV and plot these same contours on the $(\log_{10}(g_{0S}), \log_{10}(g_{1S}))$ plane for Scenarios 1 and 2 respectively. We also set $g_{0S} = g'_{0S}$, $g_{1S} = g'_{1S}$ for simplicity. Once again we see the constraints on the new Yukawa couplings are less severe for Scenario 2.
- Finally, regarding the incorporation of the current limit on $B(\mu \to e\gamma)$ from MEG experiment and its projected sensitivity into the contour plots of $B(\mu - e$ conversion) in Figs. 9–14, one can obtain the following statements
  - The plots illustrate nicely the close relation between the two CLFV processes $\mu \to e\gamma$ and $\mu - e$ conversion in nuclei using the simple formula (85) we derived in Sec. 5.

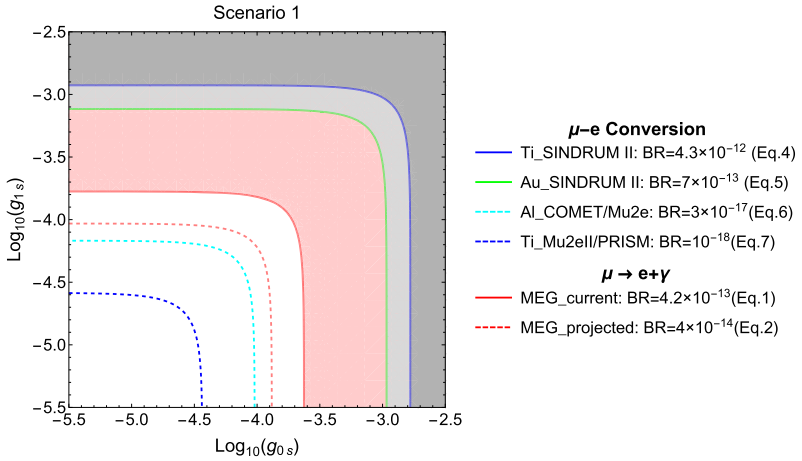

Fig. 13. Contour plots of $B(\mu - e$ conversion) and $B(\mu \to e\gamma)$ on the $(\log_{10}(g_{0S}), \log_{10}(g_{1S}))$ plane for normal mass hierarchy in Scenario 1 with $g_{0S} = g'_{0S}$, $g_{1S} = g'_{1S}$ and $M_{\text{mirror}} = 500$ GeV.

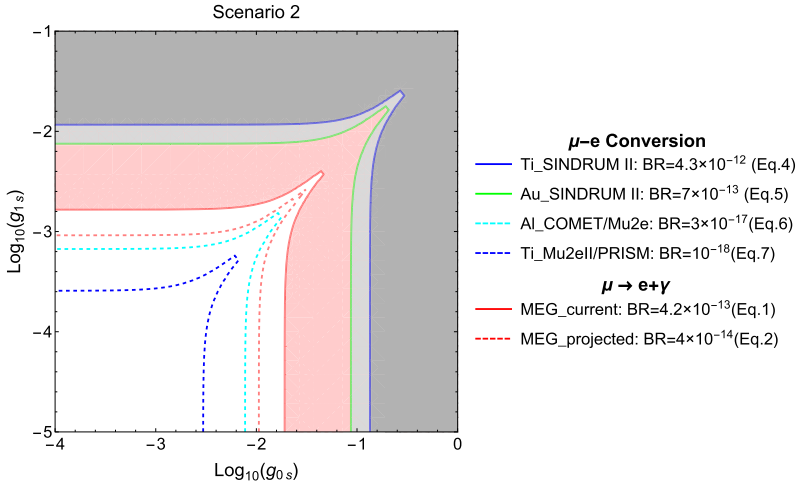

Fig. 14. Same as Fig. 13 for Scenario 2.

- In the same parameter space, $\mu \to e\gamma$ shows a tighter constraint than $\mu - e$ conversion by the fact that it excludes almost half of the searched region for the branching ratio of $\mu - e$ conversion. Therefore, our work helps narrow down future searches for $\mu - e$ conversion at Fermilab/Mu2e, J-PARC/COMET and PRISM.
- With the current upper bounds from various experiments, the radiative decay $\mu \to e\gamma$ is providing more stringent constraints on the couplings than the $\mu - e$ conversion (10^{-4} vs. 10^{-3}, about one order of magnitude better). However, for the future projected sensitivities at Mu2e and COMET, $\mu - e$ conversion is slightly more stringent, about half an order of magnitude stronger constraints on the couplings. For PRISM, it can be about an order of magnitude more stronger.

7. Summary

Mirror fermion model with electroweak scale non-sterile right-handed neutrinos is an interesting extension of the SM. Aside from its aesthetically appealing to restoring parity symmetry at higher energy scale, it can have immediate impacts for experiments in both complementary frontiers of high energy and high intensity searching for new physics of CLFV.

In this study, we discussed $\mu - e$ conversion in nuclei and radiative decay $\mu \to e\gamma$ in an extended mirror fermion model with a A_4 horizontal symmetry in the fermion and scalar sectors. We showed that the four-fermion coupling coefficients arise from the photon, Z boson, Higgses as well as gluonic and box contributions are negligibly small compared with the photon contributions to the two dipole coupling coefficients. Based on this, we established a formula relating $\mu - e$ conversion rate in nuclei to the partial decay rate of the on-shell radiative decay process $\mu \to e\gamma$.

Currently the most stringent constraint on the parameter space of the model is provided by the most recent limit on the radiative decay $\mu \to e\gamma$ from MEG. In the future, Mu2e and COMET experiments can provide more stringent constraints on the model from $\mu - e$ conversion in aluminum. The sensitivity of the new Yukawa couplings can be probed is of order 10^{-5}, about one order of magnitude improvement compared with current status from MEG. Small Yukawa couplings of order 10^{-5} or less can give rise to distinct signatures in the search of mirror charged leptons and Majorana right-handed neutrinos at the LHC (or planned colliders) in the form of displaced decay vertices with decay lengths larger than 1 mm or so [29] plus missing energies. Although unrelated to the present analysis, a similar remark can be made for the search for mirror quarks [28].

Searches for CLFV processes at low energy facilities are important and complementary to direct searches at high energy machines like the LHC for probing new physics beyond the SM.

Acknowledgements

TCY would like to thank T. N. Pham for useful discussions and the hospitality he received at Centre de Physique Théorique de l'Ecole Polytechnique where progress of this project was made. We would also like to thank Craig Group for useful comments on the manuscript. This work was supported in part by the Ministry of Science and Technology of Taiwan (MoST) under grant number 104-2112-M-001-001-MY3.

Appendix A. Formulas for $\mathcal{I}, \mathcal{J}, \mathcal{I}_{i0} (i = 1, \cdots, 5)$

In the limit of zero momentum transfer, the Feynman parameterization integrals in the various form factors defined in Secs. 4 and 5 can be carried out analytically. We collect their results here.

$$\begin{aligned}
\mathcal{I}(r) &= \frac{1}{12\,(1-r)^4}\left[-6r^2\log r + r(2r^2+3r-6)+1\right], \\
\mathcal{J}(r) &= \frac{1}{2\,(1-r)^3}\left[-2r^2\log r + r(3r-4)+1\right], \\
\mathcal{I}_{10}(r) &= \frac{1}{72\,(1-r)^6}\left[-12r^2(3+2r)\log r + (r-1)\left(3r^3+47r^2+11r-1\right)\right], \\
\mathcal{I}_{20}(r) &= \frac{1}{36\,(1-r)^5}\left[-6r^2(3+r)\log r + (r-1)\left(17r^2+8r-1\right)\right], \qquad \text{(A.90)}
\end{aligned}$$

$$\mathcal{I}_{30}(r) = \frac{1}{36\,(1-r)^4}\left[6r^3\log r + r\left(-11r^2+18r-9\right)+2\right],$$
$$\mathcal{I}_{40}(r) = \frac{1}{144\,(1-r)^6}\left[12r^3(r+4)\log r - \left(r^2-1\right)\left(37r^2-8r+1\right)\right],$$
$$\mathcal{I}_{50}(r) = \frac{1}{18\,(1-r)^5}\left[12r^3\log r - r\left(3r^3+10r^2-18r+6\right)+1\right].$$

Here r denotes the mass ratio m^2/M^2, where m and M are the masses of the scalar singlet and mirror lepton respectively. Since the masses of Higgs singlets are much smaller than those of the mirror fermions in the model, their mass ratios are really tiny. Thus to a very good approximation, we can evaluate these integrals at $r = 0$, namely $\mathcal{I}(0) = 1/12$, $\mathcal{J}(0) = 1/2$, $\mathcal{I}_{10}(0) = 1/72$, $\mathcal{I}_{20}(0) = 1/36$, $\mathcal{I}_{30}(0) = 1/18$, $\mathcal{I}_{40}(0) = 1/144$ and $\mathcal{I}_{50}(0) = 1/18$.

References

[1] S.T. Petcov, The processes mu → e gamma, mu → e e anti-e, neutrino' → neutrino gamma in the Weinberg–Salam model with neutrino mixing, Sov. J. Nucl. Phys. 25 (1977) 340, Yad. Fiz. 25 (1977) 641, Erratum: Sov. J. Nucl. Phys. 25 (1977) 698, Erratum: Yad. Fiz. 25 (1977) 1336.

[2] E. Ma, A. Pramudita, Exact formula for $(\mu \to e\gamma)$ type processes in the standard model, Phys. Rev. D 24 (1981) 1410.

[3] A.M. Baldini, et al., MEG Collaboration, Search for the lepton flavour violating decay $\mu^+ \to e^+\gamma$ with the full dataset of the MEG experiment, Eur. Phys. J. C 76 (8) (2016) 434, arXiv:1605.05081 [hep-ex].

[4] F. Renga, MEG Collaboration, Latest results of MEG and status of MEG-II, arXiv:1410.4705 [hep-ex].

[5] See the talk presented by K. Iwamoto (T2K Collaboration) at the ICHEP 2016, Chicago, August 2016.

[6] I. Esteban, M.C. Gonzalez-Garcia, M. Maltoni, I. Martinez-Soler, T. Schwetz, Updated fit to three neutrino mixing: exploring the accelerator-reactor complementarity, J. High Energy Phys. 1701 (2017) 087, arXiv:1611.01514 [hep-ph].

[7] M.C. Gonzalez-Garcia, M. Maltoni, T. Schwetz, Global analyses of neutrino oscillation experiments, Nucl. Phys. B 908 (2016) 199, arXiv:1512.06856 [hep-ph].

[8] P. Adamson, et al., NOvA Collaboration, First measurement of electron neutrino appearance in NOvA, Phys. Rev. Lett. 116 (15) (2016) 151806, arXiv:1601.05022 [hep-ex].

[9] P. Adamson, et al., NOvA Collaboration, First measurement of muon-neutrino disappearance in NOvA, Phys. Rev. D 93 (5) (2016) 051104, arXiv:1601.05037 [hep-ex].

[10] C. Dohmen, et al., SINDRUM II Collaboration, Test of lepton-flavour conservation in $\mu - e$ conversion on titanium, Phys. Lett. B 317 (1993) 631.

[11] W.H. Bertl, et al., SINDRUM II Collaboration, A search for muon to electron conversion in muonic gold, Eur. Phys. J. C 47 (2006) 337.

[12] L. Bartoszek, et al., Mu2e Collaboration, Mu2e technical design report, arXiv:1501.05241 [physics.ins-det].

[13] Y. Kuno, COMET Collaboration, A search for muon-to-electron conversion at J-PARC: the COMET experiment, PTEP 2013 (2013) 022C01.

[14] COMET Collaboration, Technical Design Report, 2016.

[15] K. Knoepfel, et al., Mu2e Collaboration, Feasibility study for a next-generation Mu2e experiment, arXiv:1307.1168 [physics.ins-det].

[16] R.J. Barlow, The PRISM/PRIME project, Nucl. Phys. Proc. Suppl. 218 (2011) 44.

[17] M. Lindner, M. Platscher, F.S. Queiroz, A call for new physics: the muon anomalous magnetic moment and lepton flavor violation, Phys. Rep. 731 (2018) 1, arXiv:1610.06587 [hep-ph].

[18] P.Q. Hung, T. Le, V.Q. Tran, T.C. Yuan, Lepton flavor violating radiative decays in EW-scale ν_R model: an update, J. High Energy Phys. 1512 (2015) 169, arXiv:1508.07016 [hep-ph].

[19] P.Q. Hung, Electroweak-scale mirror fermions, $\mu \to e\gamma$ and $\tau \to \mu\gamma$, Phys. Lett. B 659 (2008) 585, arXiv:0711.0733 [hep-ph].

[20] P.Q. Hung, A model of electroweak-scale right-handed neutrino mass, Phys. Lett. B 649 (2007) 275, arXiv:hep-ph/0612004.

[21] P.Q. Hung, T. Le, On neutrino and charged lepton masses and mixings: a view from the electroweak-scale right-handed neutrino model, J. High Energy Phys. 1509 (2015) 001, arXiv:1501.02538 [hep-ph].

[22] R. Alonso, M. Dhen, M.B. Gavela, T. Hambye, Muon conversion to electron in nuclei in type-I seesaw models, J. High Energy Phys. 1301 (2013) 118, arXiv:1209.2679 [hep-ph].
[23] D.N. Dinh, A. Ibarra, E. Molinaro, S.T. Petcov, The $\mu - e$ conversion in nuclei, $\mu \to e\gamma, \mu \to 3e$ decays and TeV scale see-saw scenarios of neutrino mass generation, J. High Energy Phys. 1208 (2012) 125, Erratum: J. High Energy Phys. 1309 (2013) 023, arXiv:1205.4671 [hep-ph].
[24] A. Abada, M.E. Krauss, W. Porod, F. Staub, A. Vicente, C. Weiland, Lepton flavor violation in low-scale seesaw models: SUSY and non-SUSY contributions, J. High Energy Phys. 1411 (2014) 048, arXiv:1408.0138 [hep-ph].
[25] A. Abada, V. De Romeri, A.M. Teixeira, Impact of sterile neutrinos on nuclear-assisted cLFV processes, J. High Energy Phys. 1602 (2016) 083, arXiv:1510.06657 [hep-ph].
[26] A. Ilakovac, A. Pilaftsis, Supersymmetric lepton flavour violation in low-scale seesaw models, Phys. Rev. D 80 (2009) 091902, arXiv:0904.2381 [hep-ph].
[27] J. Hisano, K. Tobe, Neutrino masses, muon g-2, and lepton flavor violation in the supersymmetric seesaw model, Phys. Lett. B 510 (2001) 197, arXiv:hep-ph/0102315.
[28] S. Chakdar, K. Ghosh, V. Hoang, P.Q. Hung, S. Nandi, Search for mirror quarks at the LHC, Phys. Rev. D 93 (3) (2016) 035007, arXiv:1508.07318 [hep-ph].
[29] S. Chakdar, K. Ghosh, V. Hoang, P.Q. Hung, S. Nandi, The search for electroweak-scale right-handed neutrinos and mirror charged leptons through like-sign dilepton signals, Phys. Rev. D 95 (1) (2017) 015014, arXiv:1606.08502 [hep-ph].
[30] Y. Kuno, Y. Okada, Muon decay and physics beyond the standard model, Rev. Mod. Phys. 73 (2001) 151, arXiv:hep-ph/9909265.
[31] R. Kitano, M. Koike, Y. Okada, Detailed calculation of lepton flavor violating muon electron conversion rate for various nuclei, Phys. Rev. D 66 (2002) 096002, Erratum: Phys. Rev. D 76 (2007) 059902, arXiv:hep-ph/0203110.
[32] J.C. Pati, A. Salam, Lepton number as the fourth color, Phys. Rev. D 10 (1974) 275, Phys. Rev. D 11 (1975) 703.
[33] R.N. Mohapatra, J.C. Pati, A natural left-right symmetry, Phys. Rev. D 11 (1975) 2558.
[34] G. Senjanovic, R.N. Mohapatra, Exact left-right symmetry and spontaneous violation of parity, Phys. Rev. D 12 (1975) 1502.
[35] G. Senjanovic, Spontaneous breakdown of parity in a class of gauge theories, Nucl. Phys. B 153 (1979) 334.
[36] H.B. Nielsen, M. Ninomiya, No go theorem for regularizing chiral fermions, Phys. Lett. B 105 (1981) 219.
[37] V. Hoang, P.Q. Hung, A.S. Kamat, Electroweak precision constraints on the electroweak-scale right-handed neutrino model, Nucl. Phys. B 877 (2013) 190, arXiv:1303.0428 [hep-ph].
[38] V. Hoang, P.Q. Hung, A.S. Kamat, Non-sterile electroweak-scale right-handed neutrinos and the dual nature of the 125-GeV scalar, Nucl. Phys. B 896 (2015) 611, arXiv:1412.0343 [hep-ph].
[39] H. Georgi, M. Machacek, Doubly charged Higgs bosons, Nucl. Phys. B 262 (1985) 463.
[40] M.S. Chanowitz, M. Golden, Higgs boson triplets with $M(W) = M(Z)\cos\theta_W$, Phys. Lett. B 165 (1985) 105.
[41] N. Cabibbo, Time reversal violation in neutrino oscillation, Phys. Lett. B 72 (1978) 333.
[42] L. Wolfenstein, Oscillations among three neutrino types and CP violation, Phys. Rev. D 18 (1978) 958.
[43] J. Schechter, J.W.F. Valle, Neutrino decay and spontaneous violation of lepton number, Phys. Rev. D 25 (1982) 774.
[44] W. Grimus, L. Lavoura, The seesaw mechanism at arbitrary order: disentangling the small scale from the large scale, J. High Energy Phys. 0011 (2000) 042, arXiv:hep-ph/0008179.
[45] H. Hettmansperger, M. Lindner, W. Rodejohann, Phenomenological consequences of sub-leading terms in see-saw formulas, J. High Energy Phys. 1104 (2011) 123, arXiv:1102.3432 [hep-ph].
[46] M. Blennow, E. Fernandez-Martinez, Parametrization of seesaw models and light sterile neutrinos, Phys. Lett. B 704 (2011) 223, arXiv:1107.3992 [hep-ph].
[47] E. Ma, A(4) symmetry and neutrinos, Int. J. Mod. Phys. A 23 (2008) 3366, arXiv:0710.3851 [hep-ph];
E. Ma, G. Rajasekaran, Softly broken A(4) symmetry for nearly degenerate neutrino masses, Phys. Rev. D 64 (2001) 113012, arXiv:hep-ph/0106291;
See also S.F. King, C. Luhn, Neutrino mass and mixing with discrete symmetry, Rep. Prog. Phys. 76 (2013) 056201, arXiv:1301.1340 [hep-ph], for a review and references therein.
[48] A. Zee, Group Theory in a Nutshell for Physicists, Princeton University Press, 2016, p. 289.
[49] V. Cirigliano, R. Kitano, Y. Okada, P. Tuzon, On the model discriminating power of $\mu - e$ conversion in nuclei, Phys. Rev. D 80 (2009) 013002, arXiv:0904.0957 [hep-ph].
[50] A. Corsetti, P. Nath, Gaugino mass nonuniversality and dark matter in SUGRA, strings and D-brane models, Phys. Rev. D 64 (2001) 125010, arXiv:hep-ph/0003186.
[51] H.Y. Cheng, C.W. Chiang, Revisiting scalar and pseudoscalar couplings with nucleons, J. High Energy Phys. 1207 (2012) 009, arXiv:1202.1292 [hep-ph].
[52] K. Nakamura, et al., Particle Data Group, J. Phys. G 37 (2010) 075021 and 2011 partial update for the 2012 edition.

[53] T. Suzuki, D.F. Measday, J.P. Roalsvig, Total nuclear capture rates for negative muons, Phys. Rev. C 35 (1987) 2212.
[54] G.J. Gounaris, J. Layssac, F.M. Renard, Off-shell structure of the anomalous Z and γ self-couplings, Phys. Rev. D 65 (2002) 017302, Phys. Rev. D 62 (2000) 073012, arXiv:hep-ph/0005269.
[55] C.F. Chang, P.Q. Hung, C.S. Nugroho, V.Q. Tran, T.C. Yuan, Electron electric dipole moment in mirror fermion model with electroweak scale non-sterile right-handed neutrinos, Nucl. Phys. B 928 (2018) 21, arXiv:1702.04516 [hep-ph].
[56] P.Q. Hung, Mirror fermions and the strong CP problem: a new axion-less solution, arXiv:1712.09701 [hep-ph];
P.Q. Hung, A non-vanishing neutrino mass and the strong CP problem: a new solution from the perspective of the EW-ν_R model, arXiv:1710.00498 [hep-ph];
P.Q. Hung, What does a non-vanishing neutrino mass have to say about the strong CP problem? arXiv:1704.06390 [hep-ph].